Marine Geology 395 (2018) 285–300

Contents lists available at ScienceDirect

Marine Geology

journal homepage: www.elsevier.com/locate/margo

Biostratigraphy of the last 50 kyr in the contourite depositional system of the Gulf of Cádiz

Emmanuelle Ducassou*, Rim Hassan, Eliane Gonthier, Josette Duprat, Vincent Hanquiez, Thierry Mulder

Université de Bordeaux, CNRS UMR 5805 EPOC, Allée Geoffroy St Hilaire, 33615 Pessac cedex, France

ARTICLE INFO

Editor: Michele Rebesco

Keywords:
Biostratigraphy
Foraminifera
Holocene
Younger Dryas
Heinrich Stadials
Mediterranean Outflow
Gulf of Cádiz

ABSTRACT

This paper proposes a biostratigraphic framework for the last 50 kyr in the contourite depositional system (CDS) of the Gulf of Cádiz with a solid and independent age control, and tests the reliability of faunal-based analyses in a bottom current-dominated environment related to high current velocities. The distribution of planktonic foraminifera and pteropods has been studied in twenty-two piston cores of the Holocene and Late Pleistocene age from the Gulf of Cádiz. A detailed correlation between the cores has been made possible by a large radiocarbon and isotopic data set and a high degree of similarity of frequency changes within several species by coiling direction changes of *Globorotalia truncatulinoides* and *Globorotalia hirsuta* and by occurrences of the polar species *Neogloboquadrina pachyderma* and *Limacina retroversa*. Occurrences of these polar species are clearly related to paleoclimatic oscillations and reflect rapidly changing surface water conditions in the Gulf of Cádiz during the latest Pleistocene that have been observed regardless of sedimentation rates and sedimentary environments (contouritic drifts *vs* slope without bottom current influence).

1. Introduction

Contourite depositional systems (CDS) are very common along many continental margins and in deep basins worldwide. Similar to large turbidite systems, they can reach huge lateral and vertical dimensions (*e.g.*, Heezen et al., 1966; Marani et al., 1993; Laberg et al., 1999; Stow et al., 2002; Rebesco and Camerlenghi, 2008) and have a high stratigraphic, sedimentological, paleoceanographic and paleoclimatological significance (*e.g.*, Llave et al., 2006; Voelker et al., 2006; Toucanne et al., 2007; Knutz, 2008; Bahr et al., 2015; Kaboth et al., 2015). Study of the sedimentary and stratigraphic characteristics of contourite deposits on continental margins offers the possibility of tracing the paleocirculation patterns of bottom currents and their evolution through time. Bottom currents are the result of both thermohaline and wind-driven circulation of the ocean (*e.g.*, Rebesco and Camerlenghi, 2008), they are highly sensitive to climate changes and a reliable, highly resolved stratigraphic framework is required to constrain their impact on continental margins. However, in such a dynamic depositional environment, carbonate tests of planktonic and benthic fauna classically used for accurate stratigraphical analyses (*e.g.*, $\delta^{18}O$, ^{14}C) can be missing or concentrated, resulting in potentially discontinuous and unreliable records.

Biostratigraphic events can be an interesting tool in such environments as their evaluation requires relatively few specimens (≥ 300) compared to, for example, radiocarbon datings. In the North Atlantic, the percentages of *Neogloboquadrina pachyderma*, previously known as *N. pachyderma* sinistral (Darling et al., 2006), a polar species of planktonic foraminifera, are often given to characterize brief cold climatic phases such as the Heinrich Stadials (Heinrich, 1988; Darling et al., 2006; Eynaud et al., 2009; Voelker and de Abreu, 2011) in spite of their low abundance (a few percent) at mid and low latitudes. In this paper, we want to show that other species offer the same kind of precision during periods described as relatively homogeneous in faunal assemblages, such as the Holocene. Those bio-events allow rapid correlations between nearby sedimentary cores. Because the Gulf of Cádiz is a reference area for the study of the impact of bottom currents on local sedimentation, it would be worth questioning if the use of stratigraphical methods based on microfauna, potentially displaced or reworked by those bottom currents, is reliable. Bottom currents are semi-permanent features of deep ocean circulation and they are characterized by strong spatiotemporal variations in their velocity. In the CDS of the Gulf of Cádiz, the Mediterranean Outflow Water (MOW) mean velocities commonly reach ~80 cm/s implying transport of sand and severe winnowing (Hernández-Molina et al., 2011).

This study aims (1) to describe the main bio-events recognized during the last 50 kyr in the Gulf of Cádiz and to discuss their age based

* Corresponding author at: Université de Bordeaux, CNRS UMR 5805 EPOC, Allée Geoffroy St Hilaire, 33615 Pessac cedex, France.
E-mail address: emmanuelle.ducassou@u-bordeaux.fr (E. Ducassou).

https://doi.org/10.1016/j.margeo.2017.09.014
Received 25 July 2016; Received in revised form 2 September 2017; Accepted 28 September 2017
Available online 16 October 2017
0025-3227/

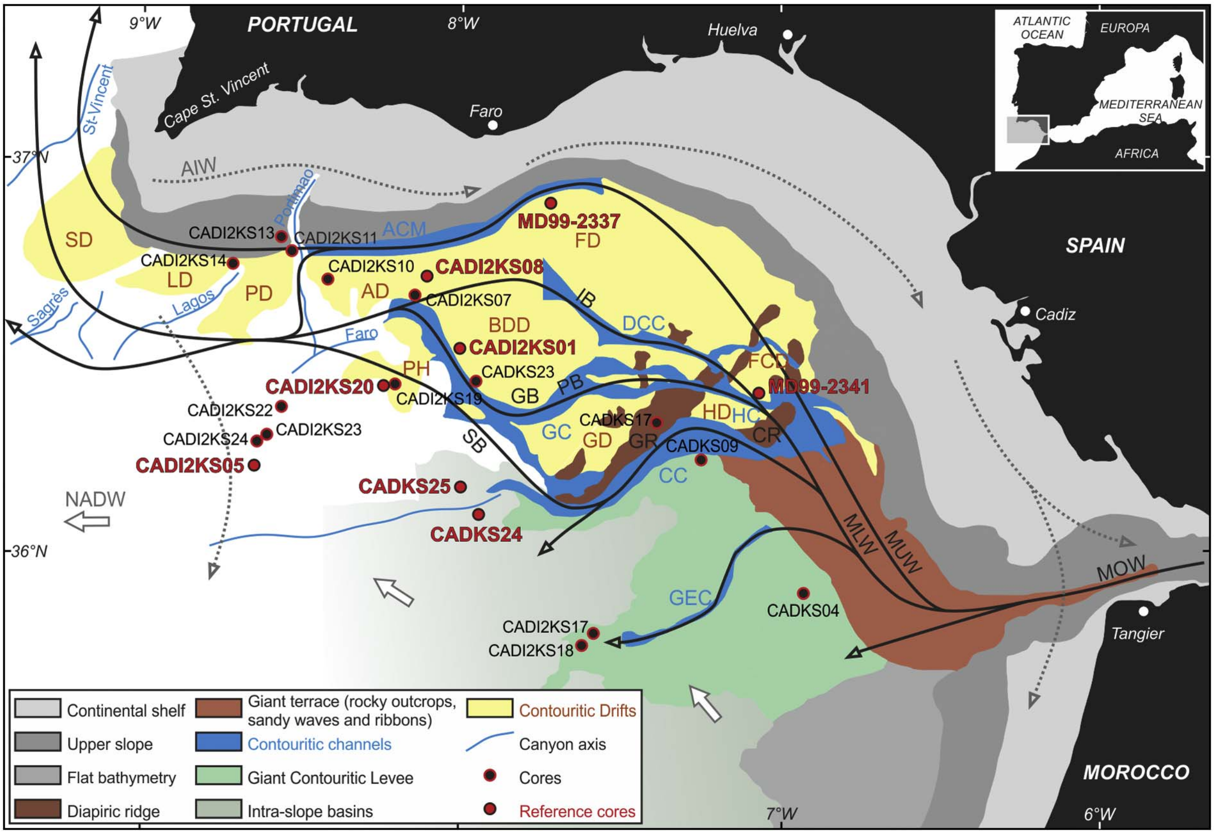

Fig. 1. Map of the Gulf of Cadiz showing the general circulation pattern of the water masses (grey and black arrows) and the main morphosedimentary sectors of the Contourite Depositional System (Hernández-Molina et al., 2006). Black and red dots are the locations of cores used in this study. AIW: Atlantic Inflow Water; NADW: North Atlantic Deep Water; MOW: Mediterranean Outflow Water; MUW: Mediterranean Upper Water; MLW: Mediterranean Lower Water; IB: Intermediate MLW Branch; PB: Principal MLW Branch; SB: Southern MLW Branch; AD: Albufeira Drift; BDD: Bartolome Dias Drift; FD: Faro Drift; FCD: Faro-Cadiz Drift; GD: Guadalquivir Drift; HD: Huelva Drift; PD: Portimao Drift; PH: Portimao High; LD: Lagos Drift; SD: Sagrès Drift; CR: Cadiz Ridge; GB: Guadalquivir Bank; GR: Guadalquivir Ridge; ACM: Alvarez Cabral Moat; CC: Cadiz Channel; DCC: Diego Cao Channel; GC: Guadalquivir Channel; GEC: Gil Eanes Channel; HC: Huelva Channel (modified from Hanquiez, 2006 and Hernández-Molina et al., 2003, 2006). (For interpretation of the references to colour in this figure legend, the reader is referred to the web version of this article.)

on oxygen and radiocarbon isotope data, and (2) to evaluate the reliability of the identified regional bio-events based on twenty-one cores collected in different areas under and out of the influence of the high-velocity bottom currents in the Gulf of Cádiz.

2. Regional setting

The Gulf of Cádiz is located southwest of the Iberian Peninsula, west of the Strait of Gibraltar (Fig. 1). It is the primary site of water mass exchange between the Atlantic Ocean and the Mediterranean Sea through the Strait of Gibraltar. Whereas the fresher and colder Atlantic Inflow Water (AIW) enters the Mediterranean at the surface, the relatively dense, warm and saline waters from Mediterranean (Levantine Intermediate Water, LIW and Western Mediterranean Deep Water, WMDW) flow westward to form the Mediterranean Outflow Water (MOW; Bryden and Stommel, 1982; Junglaus and Mellor, 2000). Two separate flow cores are recognized from 300 to 600 m (Mediterranean Upper Water, MUW; Ambar and Howe, 1979; Ambar et al., 1999; O'Neil-Baringer and Price, 1999) and from 600 to 1500 m (Mediterranean Lower Water, MLW; Madelain, 1970; Zenk and Armi, 1990; Rogerson et al., 2005, Stow et al., 2013; Fig. 1). At approximately 7°W, the MLW is subdivided into three branches named the Intermediate Branch (IB), Principal Branch (PB) and Southern Branch (SB) from North to South (Madelain, 1970; Kenyon and Belderson, 1973; Nelson et al., 1993; Fig. 1). Below water depths of 1200 m and 1500 m in the eastern and western parts of the Gulf, respectively, the MOW is disconnected from the seafloor and underlain by the North Atlantic Deep Water (NADW) (O'Neil-Baringer and Price, 1999; Hernández-Molina et al., 2003, 2011).

In the present day, MOW velocities range from 2.5 m/s in the Strait of Gibraltar to 20–10 cm/s in the MUW and MLW at Cape St. Vincent. These velocities are typically 80 to 40 cm/s in MUW and 50 to 30 cm/s in the three MLW branches from SE to NW in the Gulf of Cádiz (Boyum, 1967; Habgood et al., 2003; Hanquiez et al., 2007). Those bottom currents are semi-permanent and have a net alon- slope flow motion but can be extremely variable in direction and velocities (Stow and Faugères, 2008; Stow et al., 2013). Such energetic flows are able to erode, transport and deposit sediments on the sea floor, and the interaction of MOW with the slope generates a large contourite depositional system (Hernández-Molina et al., 2006; Fig. 1).

The northwestern part of the Gulf of Cádiz is largely dominated by contouritic drifts such as separated mounded drifts (Faro-Albufeira drifts; Fig. 1) and sheeted drifts (Bartolome Dias, Huelva, Guadalquivir, Portimão, Lagos and Sagres drifts; Faugères et al., 1984, 1994; Gonthier et al., 1984; Stow et al., 1986; Marchès et al., 2007; Fig. 1).

Contouritic channels are also important features in the Gulf of Cádiz as they result from both erosive action of bottom currents and neotectonic activity (*e.g.*, deformation and diapiric intrusion). Stow et al. (2013) show that bedforms observed in contourite channels are related to high-energy flows, such as channelized MOW branches but can also be related to amplification of tidal or meteorological-induced bottom currents (internal tides and internal waves). The Cádiz, Guadalquivir, Huelva and Diego Cao channels are the four largest contouritic channels of the area (Fig. 1).

Table 1
Details of cores used during this study.

Core	Latitude	Longitude	Depth (m)	Length (m)	Cruise
CADKS04	35.882	− 6.9262	814	6.2	CADISAR
CADKS07	36.0271	− 7.3111	1006	4.71	CADISAR
CADKS09	36.2183	− 7.2432	814	3.53	CADISAR
CADKS17	36.3252	− 7.3845	852	8.75	CADISAR
CADKS23	36.4396	− 7.9212	737	2.22	CADISAR
CADKS24	36.0824	− 7.9421	1316	8.65	CADISAR
CADKS25	36.1508	− 8.0015	1259	7.52	CADISAR
CADI2KS01	36.5	− 8.0000	820	5.65	CADISAR 2
CADI2KS05	36.2083	− 8.6533	1949	7.62	CADISAR 2
CADI2KS07	36.6477	− 8.1417	786	4.87	CADISAR 2
CADI2KS08	36.6815	− 8.104	789	5.4	CADISAR 2
CADI2KS10	36.6788	− 8.4016	703	2.85	CADISAR 2
CADI2KS11	36.7538	− 8.5272	938	2.82	CADISAR 2
CADI2KS13	36.78	− 8.5633	672	2.88	CADISAR 2
CADI2KS14	36.7133	− 8.7117	752	4.71	CADISAR 2
CADI2KS17	35.7808	− 7.585	1446	1.76	CADISAR 2
CADI2KS20	36.4117	− 8.2358	1103	3.25	CADISAR 2
CADI2KS22	36.3566	− 8.5536	2555	3.66	CADISAR 2
CADI2KS23	36.2833	− 8.61	2254	7.3	CADISAR 2
CADI2KS24	36.27	− 8.6367	2129	6.75	CADISAR 2
MD99-2337	36.867	− 7.717	598	19.88	IMAGES V
MD99-2341	36.3892	− 7.0657	582	19.42	IMAGES V

3. Material

This study is based on twenty-two cores collected in the Gulf of Cádiz during three cruises (Table 1). Among them, eight cores that provide seemingly continuous records from a wide range of depositional environments have been chosen as reference cores.

Two long piston cores, MD99-2337 and MD99-2341, were collected by the *r/v Marion Dufresne II* (IPEV) during the IMAGES V/GINNA cruise (1999; Fig. 1; Table 1). They are located in the Faro (MD99-2337) and the Faro-Cádiz (MD99-2341) drifts. These locations are presently under the influence of the MUW and the MLW, respectively (Hernández-Molina et al., 2006; Llave et al., 2006).

Two Küllenberg cores were recovered by the *r/v Le Suroît* (IFREMER) during the CADISAR 1 cruise (2001; Fig. 1; Table 1). Core CADKS24, located on a small plateau, and core CADKS25, collected in the Lolita mud volcano (Somoza et al., 2003) are both at the limit of the influence of the SB.

Four Küllenberg cores were recovered by the *r/v Le Suroît* (IFREMER) during the CADISAR 2 cruise (2004; Fig. 1; Table 1): (i) CADI2KS01 in the Bartolome Dias Drift under the influence of the PB, (ii) CADI2KS20 in the Portimao High, under the influence of the SB, (iii) CADI2KS08 in the Albufeira Drift under the influence of the IB, and (iv) CADI2KS05 westward of the Albufeira High and out of the influence of the MOW.

4. Methods

The cores MD99-2337, CADI2KS01, CADI2KS08, and CADI2KS20 were sampled every 10 cm for analyses of oxygen isotopes and biostratigraphy. The longest core MD99-2341 was sampled every 5 cm for the same purposes, to gain a greater resolution. The cores CADI2KS05, CADKS24 and CADKS25 and all the other cores of this study were sampled every 10 cm for biostratigraphic analyses. Visual description and X-ray images have been used during sampling to avoid the largest bioturbations. The samples were washed and sieved to remove material finer than 63 µm, using demineralised water for the last rinse. The residues were dried and weighed and the > 150-µm fraction was separated for foraminiferal counts.

4.1. Isotope and radiometric analyses

Stable oxygen measurements were carried out on 10 to 15 visually clean specimens of the planktonic foraminifera *Globigerinoides ruber alba*, *Globigerina bulloides*, *Neogloboquadrina incompta* (previously known as *N. pachyderma* dextral; Darling et al., 2006), depending on their presence from all reference cores, ~3 specimens of the benthic foraminifera *Uvigerina peregrina* and *Uvigerina mediterranea* for core MD992337. Specimens have been handpicked in the > 250 µm size fraction for planktonic foraminifera and > 150 µm for benthic foraminifera. Measurements were made at Bordeaux University, UMR 5805 EPOC, using an *Optima Micromass* mass spectrometer. External reproducibility for standards on this mass-spectrometer is ± 0.048‰. For core MD99-2341, isotopic analyses were carried out in the isotope laboratory at Bremen University with a CARBO KIEL automated carbonate preparation device linked on-line to a FINNIGAN MAT 252 mass spectrometer, with a long-term reproducibility of 0.08‰ (Mulder et al., 2002; Toucanne et al., 2007).

Radiocarbon datings have been performed on 112 samples, corresponding to > 10 mg of visually clean handpicked planktonic foraminifera from the > 150-µm fraction (Tables 2a and 2b). For measurements made on 'bulk' samples, different species of planktonic foraminifera were handpicked. Samples were treated in 2 mL of 0.01 M nitric acid for 15 min to remove organic coatings. Afterwards, samples were dried under vacuum and then digested in phosphoric acid at 60 °C until 1 mg of carbon was produced as CO_2. The CO_2 was reduced with H_2 in the presence of iron at 600 °C to graphite and pressed directly onto a target. The activity of ^{14}C in the graphite targets was measured on an accelerator mass spectrometer (AMS) and standardized using an in-house CO_2 standard HOxI that was normalized to a $\delta^{13}C$ value of − 25‰. The ^{14}C activity was corrected for fractionation in the mass spectrometer based on the $\delta^{13}C$ measurement. Radiocarbon ages were determined at the Laboratoire de Mesure du Carbone 14-Saclay (Paris) thanks to the French Artemis programme, and at the Leibniz-Labor Radiometric Dating and Isotope Research (Kiel University) for core MD99-2341 (Tables 2a and 2b).

Radiocarbon ages were calibrated to calendar years by using the web-based Calib Rev. 7.0.2 program/Marine13 data set (Stuiver and Reimer, 1993; Reimer et al., 2009). Ages indicated correspond to the median probability of the probability distribution (Telford et al., 2004).

4.2. Faunal analyses

The > 150-µm fraction was split into aliquots of at least 250 specimens of planktonic foraminifera for identification, according to the taxonomy of Hemleben et al. (1983), Kennett and Srinivasan (1983), Bolli et al. (1989), Darling et al. (2006), Spezzaferri et al. (2015). Special focus has been given to the species *Neogloboquadrina pachyderma*, *Globorotalia truncatulinoides*, *Globorotalia hirsuta*, *Globigerinoides ruber rosea*, *Globigerinoides conglobatus*, *Globorotalia crassaformis* and *Trilobatus sacculifer*.

N. pachyderma is a polar species, which is typically used in temperate latitudes to identify the presence of subpolar to polar surface waters and cold climatic episodes such as the Heinrich Stadials (Schiebel et al., 2001; Darling et al., 2006; Eynaud et al., 2009; Voelker et al., 2009; Voelker and de Abreu, 2011). The data of *N. pachyderma* are given as percentages of the total planktonic foraminiferal number.

Gs. ruber rosea, *Gs. conglobatus*, *Gr. crassaformis* and *T. sacculifer* are tropical and subtropical species and are typically present in warm periods such as the Holocene and the Bølling-Allerød (B-A). Their semi-quantitative abundance is used to indicate the boundaries of the Holocene and the B-A (vA ≥ 30%; Abundant = 15–30%; Common = 5–15%; Few = 1–5%; Barren = none observed; Sierro et al., 1999; De Abreu et al., 2003; Rogerson et al., 2005).

Gr. hirsuta is a subtropical species which has been previously used as a stratigraphical marker, rather than a paleoclimatic marker. Despite the scarcity of this species in sediments, the change in its coiling direction has been already used to identify the Pleistocene-Holocene boundary along the Iberian margins (*e.g.*, Pujol, 1975; Duprat, 1983;

Table 2a
Radiocarbon ages of cores of this study. LLRDIR: Leibniz-Labor Radiometric Dating and Isotope Research. Bulk: surface-dwelling planktonic foraminifera.

Core	Depth (cm)	Lab code	Species	Conventional AMS ^{14}C age (^{14}C yr BP)	Standard error	95,4% (2 sigma) cal yr BP age ranges	Cal yr BP age median probability	Remarks
CADI2KS01	1	SacA 21252	Bulk	930	± 30	486–608	530	
	31	SacA 21253	Bulk	1870	± 30	1332–1509	1416	
	71	SacA 11184	*Gs. ruber alba*	3395	± 30	3169–3352	3266	
	91	SacA 6458	*Gr.inflata*	5435	± 35	5715–5898	5810	
	101	SacA 6459	*Gr.inflata*	5780	± 80	5986–6360	6194	
	121	SacA 21255	Bulk	7830	± 30	8202–8368	8304	
	bis	SacA 21254	Bulk	8190	± 30	8570–8811	8677	
	135	SacA 17191	*Gr.inflata*	9705	± 50	10,477–10,747	10.606	
	151	SacA 10613	*Gs. ruber alba*	9480	± 35	10,219–10,444	10.321	
	201	SacA 10614	*Gr.inflata*	12.950	± 45	14,504–15,123	14.863	
	215	SacA 21256	Bulk	14.065	± 45	16,254–16,698	16.465	
	261	SacA 17192	*Gr.inflata*	14.650	± 60	17,126–17,547	17.349	
	316	SacA 21257	Bulk	19.000	± 70	22,320–22,634	22.460	
	371	SacA 10615	*Gr.inflata*	20.350	± 90	23,727–24,266	24.001	
	421	SacA 10616	*G.bulloides*	22.060	± 80	25,764–26,077	25.919	
	455	SacA 10617	*G.bulloides*	24.290	± 100	27,700–28,182	27.916	
	471	SacA 10618	*G.bulloides*	25.450	± 120	28,762–29,432	29.080	
	521	SacA 10619	*Gr.inflata*	30.810	± 200	34,006–34,766	34.390	
CADI2KS05	1	SacA 17193	*Gs.ruber alba*	1055	± 30	551–672	627	
	11	SacA 19761	Bulk	985	± 30	517–634	576	
	91	SacA 19762	Bulk	4085	± 30	4002–4234	4127	
	211	SacA 17194	*Gs.ruber alba*	8475	± 40	8987–9228	9088	
	251	SacA19763	Bulk	10.045	± 35	10,898–11,168	11.056	
	271	SacA19764	Bulk	12.255	± 50	13,537–13,871	13.717	
	301	SacA19765	Bulk	12.230	± 60	13,497–13,853	13.687	
	341	SacA19766	Bulk	14.160	± 45	16,380–16,871	16.619	
	381	SacA19767	Bulk	15.150	± 50	17,761–18,112	17.943	
CADI2KS07	1	SacA 21258	Bulk	835	± 30	417–517	472	
	13	SacA 22375	Bulk	1150	± 30	645–761	696	
	61	SacA 21259	*Gs.ruber* + *Gr.inflata*	3955	± 30	3847–4060	3945	
	101	SacA 6460	*Gr.inflata*	5480	± 35	5742–5935	5862	
	181	SacA 21260	bulk	8285	± 35	8691–8974	8843	
	241	SacA 21261	bulk	10.170	± 40	11,074–11,255	11.170	
	281	SacA 6461	*Gr.inflata*	12.640	± 40	13,948–14,341	14.133	
CADI2KS08	51	SacA 10620	*Gr.inflata*	3085	± 30	2762–2943	2851	
	91	SacA 10621	*Gr.inflata*	7835	± 35	8200–8375	8307	Discarded: reworked sediment
	101	SacA 6462	*Gr.inflata*	4765	± 30	4882–5142	5013	
	121	SacA 10622	*Gr.inflata*	5620	± 30	5914–6123	6013	
	212	SacA 10623	*Gr.inflata*	7985	± 30	8371–8523	8438	
	271	SacA 10624	*Gr.inflata*	9365	± 40	10,120–10,294	10.201	
	307	SacA 10625	*Gr.inflata*	10.160	± 40	11,063–11,247	11.163	
	326	SacA 10626	*Gr.inflata*	11.030	± 40	12,493–12,675	12.584	
	351	SacA 10629	*Gr.inflata*	12.820	± 70	14,154–14,934	14.515	
	355	SacA 17196	*Gr.inflata*	12.900	± 50	14,313–15,051	14.720	
	366	SacA 10627	*Gr.inflata*	12.815	± 40	14,181–14,804	14.487	On the basis of planktonic $\delta^{18}O$ record assumed to be too young
	435	SacA 10628	*Gr.inflata*	14.890	± 50	17,479–17,867	17.656	
	503	SacA 17197	*Gr.inflata*	16.960	± 80	19,696–20,209	19.973	
CADI2KS10	6	SacA 10713	*Gr.inflata*	4645	± 30	4804–4954	4862	
	21	SacA 6466	*Gr.inflata*	19.580	± 220	22,544–23,621	23.103	
	70	SacA 6467	*Gr.inflata*	40.760	± 630	42,908–45,035	43.943	Discarded: likely reworked sediment
	131	SaA 17187	*Gr.inflata*	54.000	± 2500			Discarded: likely reworked sediment
	261	SaA 17188	*Gr.inflata*	52.000	± 1900			Discarded: likely reworked sediment
	286	SacA 6468	*Gr.inflata*	14.740	± 60	17,231–17,662	17.470	Discarded: likely contaminated sample
CADI2KS11	82	SacA 17190	*Gr.inflata*	8610	± 40	9131–9395	9276	
	249	SacA 11187	*Gs. ruber alba*	10.195	± 40	11,096–11,276	11.188	

Sierro et al., 1999).

Gr. truncatulinoides is also a subtropical species but can be found in a broad suite of environments, except for the polar provinces and areas with extreme salinity (Ericson and Wollin, 1968; Bé and Tolderlund, 1971; Bé, 1977; Hemleben et al., 1983). It is considered as a deep-dwelling species (Bé, 1960; Hemleben et al., 1985; Lohmann and Schweitzer, 1990) that lives preferentially in phosphate- and nutrient-rich waters and is therefore a good indicator of thermocline location (Mulitza et al., 1999; Cléroux et al., 2009). Sinistral forms seem to live in a deeper thermocline than dextral specimens (Lohmann and Schweitzer, 1990; Ujiié et al., 2010). The data of *Gr. truncatulinoides* are given as percentages of coiling ratio, using the following formula:

Table 2b
Radiocarbon ages of cores of this study. LLRDIR: Leibniz-Labor Radiometric Dating and Isotope Research. Bulk: surface-dwelling planktonic foraminifera.* corresponds to *G. bulloides* or *Gr. ruber alba* or pteropod *Clio* sp. or *Cavolinia* sp. (Llave et al., 2006).

Core	Depth (cm)	Lab code	Species	Conventional AMS ^{14}C age (^{14}C yr BP)	Standard error	95,4% (2 sigma) cal yr BP age ranges	Cal yr BP age median probability	Remarks
CADI2KS13	254	SacA 17189	*G.bulloides*	1535	± 30	991–1176	1094	
CADI2KS14	11	SacA 10711	*Gr.inflata*	4165	± 30	4136–4369	4244	
	29	SacA 6469	*Gr.inflata*	12.310	± 50	13,615–13,941	13.781	
CADI2KS17	7	SacA 17178	*Gs.ruber alba*	1710	± 35	1182–1332	1267	
	40	SacA 17185	*Gr.inflata*	1540	± 35	983–1191	1099	
	90	SacA 17179	*G.bulloides*	6000	± 45	6296–6525	6412	
CADI2KS19	131	SacA 17183	*N. incompta*	30.340	± 210	33,668–34,427	34.019	
	221	SacA 17184	*G.bulloides*	33.230	± 290	36,136–37,915	36.869	
CADI2KS20	21	SacA 10629	*Gs. ruber alba*	5640	± 30	5939–6154	6041	
	41	SacA 10630	*Gs. ruber alba*	7960	± 30	8351–8503	8414	
	106	SacA 10631	*Gs. ruber alba*	12.230	± 40	13,526–13,830	13.690	
	131	SacA 10632	*Gr.inflata*	12.755	± 45	14,116–14,688	14.349	
	142	SacA 10633	*G.bulloides*	14.760	± 50	17,288–17,674	17.498	On the basis of planktonic $\delta^{18}O$ record assumed to be too old
	171	SacA 10634	*G.bulloides*	14.520	± 50	16,972–17,407	17.176	
	211	SacA 10635	*Gr.inflata*	16.460	± 50	19,203–19,559	19.383	
	282	SacA 10636	*Gr.inflata*	18.350	± 60	21,524–21,938	21.745	
	296	SacA 17186	*Gr.inflata*	19.020	± 90	22,301–22,713	22.479	
CADI2KS22	160	SacA 17176	*Gr.inflata*	7745	± 45	8102–8331	8220	
CADI2KS23	211	SacA 17177	bulk	8440	± 40	8955–9195	9048	
CADI2KS24	11	SacA 22365	*Gs.ruber alba*	620	± 30	140–331	269	
	281	SacA 22366	*Gr.inflata*	8510	± 30	9019–9247	9134	
	321	SacA 22367	*Gr.inflata*	10.070	± 30	10,950–11,183	11.085	
	361	SacA 22368	*Gr.inflata*	10.810	± 35	12,082–12,488	12.301	
	381	SacA 22369	*Gr.inflata*	11.625	± 35	12,977–13,243	13.122	
	401	SacA 22370	*Gr.inflata*	12.070	± 40	13,384–13,658	13.509	
	451	SacA 22371	*Gr.inflata*	12.945	± 40	14,516–15,114	14.857	
	471	SacA 22372	*Gr.inflata*	13.300	± 40	15,216–15,604	15.391	
	501	SacA 22373	bulk	14.190	± 50	16,423–16,925	16.671	
	531	SacA 22374	bulk	15.165	± 45	17,795–18,125	17.959	
CADKS04	83	SacA 17204	*Gr.inflata*	10.385	± 45	11,241–11,719	11.450	
	162	SacA 002293	*G.bulloides*	14.720	± 80	17,158–17,670	17.440	
	254	SacA 002294	*Gr.inflata*	9590	± 60	10,268–10,617	10.463	On the basis of biostratigraphic framework assumed to be too young
	405	SacA 10715	*Gr.inflata*	30.040	± 170	33,504–34,103	33.802	
	463	SacA 002295	*Gs.ruber alba*	18.500	± 110	21,612–22,268	21.934	On the basis of biostratigraphic framework assumed to be too young
CADKS07	63	SacA 17206	*Gr.inflata*	11.37	± 50	12,685–12,964	12.826	
CADKS09	125	SacA 17207	*Gs. ruber alba*	8660	± 40	9221–9440	9337	
CADKS17	36	SacA 17205	*Gs. ruber alba*	2110	± 30	1593–1796	1691	
	141	SacA 001828	*Gr.inflata*	6270	± 50	6603–6865	6723	
	528	SacA 17198	*Gs. ruber alba*	10.585	± 45	11,625–12,078	11.881	
CADKS23	176	SacA 17199	*Gr.inflata*	30.740	± 210	33,948–34,728	34.337	
CADKS24	215	SacA 001831	*Gs. ruber alba*	10.490	± 70	11,323–11,968	11.657	
	378	SacA17200	*Gr.inflata*	12.930	± 60	14,356–15,110	14.796	
	527	SacA 17201	*N. incompta*	15.430	± 70	18,021–18,462	18.256	
CADKS25	6	SacA 17202	*Gr.inflata*	1295	± 30	758–915	841	
	101	SacA 17203	*Gs. ruber alba*	9590	± 50	10,285–10,596	10.466	
MD 99-2341	5	KIA14636	*	1585	± 25	1062–1228	1151	
	65	KIA14637	*	5845	± 35	6180–6344	6263	
	255	KIA14638	*	9120	± 50	9679–10,097	9868	
	370	KIA14639	*	11.130	± 50	12,555–12,741	12.643	
	485	KIA14640	*	14.210	± 80	16,391–16,992	16.701	
	565	KIA14641	Pteropod shell	15.010	± 110	17,500–18,043	17.78	
	580	KIA14642	*	15.720	± 100	18,351–18,789	18.585	
	755	KIA14643	*	20.940	± 130	24,335–25,161	24.731	
	805	KIA14644	*	21.530	± 190	25,018–25,856	25.46	
	1005	KIA14645	*	26.290	± 240	29,491–30,717	30.112	
	1285	KIA14646	*	32.040	± 560	34,419–36,721	35.541	
	1435	KIA14647	*	33.250	± 570	35,681–38,455	37.008	

%GTS = GTS ∗ 100 / (GTS + GTD) where GTS is the number of specimens of *Gr. truncatulinoides* sinistral and GTD the number of specimens of *Gr. truncatulinoides* dextral. This coiling ratio has been calculated only when the number of *Gr. truncatulinoides* represented at least 2% of the total assemblage.

The pteropod species *Limacina retroversa* is an epiplanktonic subarctic species that lives in a temperature range of 2–19 °C (optimum 7–12 °C, Bé and Gilmer, 1977; Janssen, 2006). This species, as well as the other pteropods, are well preserved without evidence of dissolution in the studied samples. All specimens have been counted in each sample and they are indicated in the following results as the number of specimens per gram of sediment. Pteropod fragments have been counted only when more than half of the specimen was observed.

4.3. Sedimentological analyses

The sedimentological study is based on visual description, X-ray images, and measurements of carbonate content. Grain-size analyses have been performed with a laser microgranulometer Malvern MASTERSIZER S (University of Bordeaux, UMR 5805 EPOC) using the median grain size (D50). This parameter has been chosen because it shows very similar variations to the 10–63-μm fraction and is referred to as the current-speed indicator (McCave et al., 1995). However, it represents the whole grain-size fraction. Carbonate content was measured using a Bernard calcimeter. It is indicated in the synthetic core logs by white (> 30%) and grey colours (< 30%).

5. Results: chronological and biostratigraphical framework of the Gulf of Cádiz over the last 50 kyr

Planktonic and benthic foraminiferal $\delta^{18}O$ curves, radiocarbon datings and biostratigraphical data for cores CADI2KS05, CADKS24, CADKS25, MD99-2341, MD99-2337, CADI2KS08, CADI2KS01, and CADI2KS20 are shown in Figs. 2 to 5 and Tables 2a and 2b. Correlations have been made between these records on the basis of a series of ten events recognized in planktonic foraminiferal and pteropod assemblages and in $\delta^{18}O$ data.

5.1. Isotopic data

The chronostratigraphy of the eight reference cores is primarily based on AMS radiocarbon datings and $\delta^{18}O$ records. The stable oxygen isotopic composition of calcareous tests was determined for *G. bulloides*, *Gs. ruber* and *N. incompta* (planktonic); and *U. peregrina* and *U. mediterranea* (benthic). In our record, the range of planktonic $\delta^{18}O$ values is − 1.10 to 2.68‰ *versus* PDB and of benthic $\delta^{18}O$ values is 0.9 to 4.5‰ (Figs. 3 to 5). These values are in agreement with the nearby core MD99-2339 (Voelker et al., 2006, 2009). Planktonic and benthic $\delta^{18}O$ data show the same trends with relatively similar and high values during Heinrich events and lower values during warmer intervals (MIS3, Last Glacial Maximum - LGM, B-A, and Holocene). The greatest $\delta^{18}O$ values are recorded at the beginning of the H1 and H2 events (Figs. 3 to 5). The planktonic $\delta^{18}O$ curves show greater amplitude as a local signal is superimposed on the global oxygen isotope trend observed through the benthic $\delta^{18}O$ data (Fig. 4). Toucanne et al. (2007) correlated the $\delta^{18}O$ signal of core MD99-2341 with the GISP2 ice core record, and showed the millennial-scale variability (Daansgard-Oeschger Interstadial/Stadial cycles; Fig. 3). This core goes as far back as 50 kyr, and its excellent correlation to the Greenland ice core record is interesting for the comparison of the timing of our regional archives to more global ones.

The age models of these cores for the last 50 kyr are presented in Fig. 6 (tie-points from Tables 2a, 2b and 3). As known from previous works, sedimentation rates are not steady, ranging from ~8 to ~110 cm/kyr. For cores under the influence of the MOW, sedimentation rates globally increase during H1 (> 20 cm/kyr) but decrease during the Younger Dryas and the Holocene (Figs. 3 to 6). For the shallowest core, which is also the closest to the Iberian coast (MD99-2337; Fig. 4; Table 3), sedimentation rates are higher during the LGM (≥ 110 cm/kyr).

5.2. Biostratigraphical results

5.2.1. Holocene and Bølling-Allerød assemblages

G. rosea, *Gs. conglobatus*, *Gr. crassaformis*, and *T. sacculifer* are typically present during interglacial periods and more precisely the Holocene period in this study area. The first co-occurrence of these four species over the last 50 kyr is observed at 11,657 cal yr BP in core

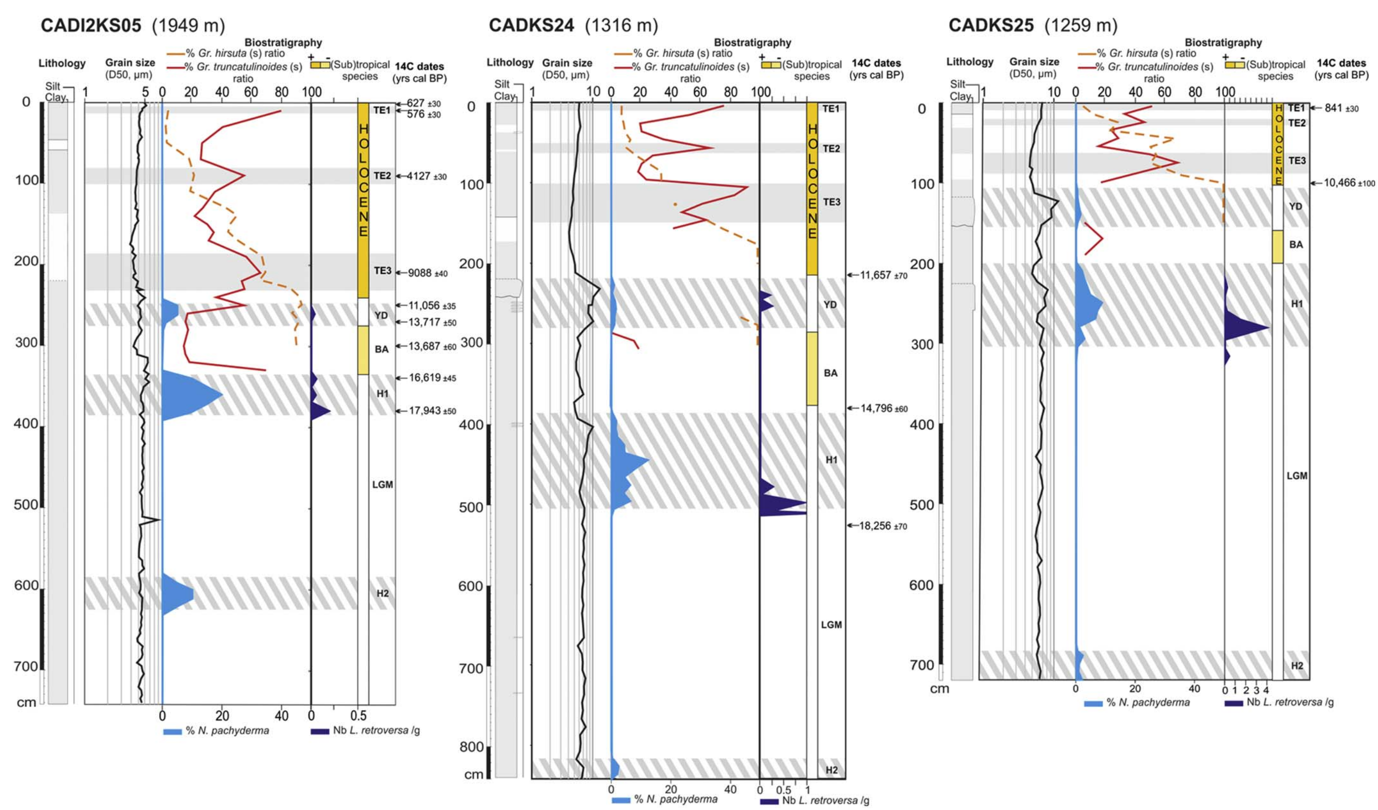

Fig. 2. Stratigraphical synthesis of the cores CADI2KS05, out of MOW influence, CADKS24 and CADKS25, located at the limit of influence of the Southern Branch (MLW). From left to right: core log (grey: < 30% $CaCO_3$; white: > 30% $CaCO_3$), grain-size data, biostratigraphical curves of planktonic foraminifera and pteropods, and radiocarbon datings. TE1 to TE3: *Gr. truncatulinoides* (s) events, YD: Younger Dryas, BA: Bølling-Allerød, H1 to H2: Heinrich Stadials; LGM: Last Glacial Maximum.

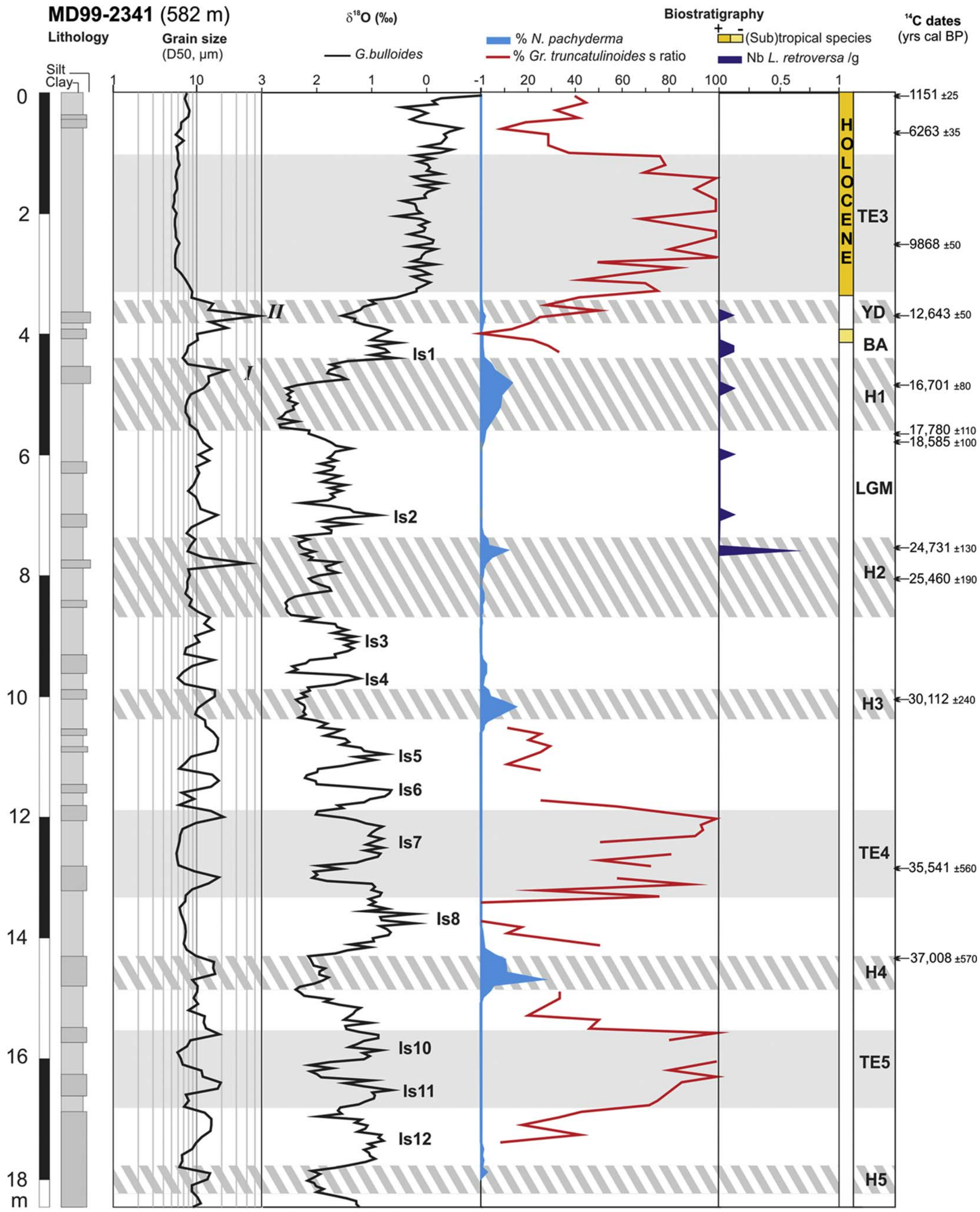

Fig. 3. Stratigraphical synthesis of the core MD99–2341, located under the MLW influence. From left to right: core log (grey: < 30% $CaCO_3$), grain-size data, $\delta^{18}O$ planktonic curve, biostratigraphical curves of planktonic foraminifera and pteropods, and radiocarbon datings. TE3 to TE5: *Gr. truncatulinoides* (s) events, YD: Younger Dryas, BA: Bølling-Allerød, H1 to H4: Heinrich Stadials; LGM: Last Glacial Maximum. Is1 to Is12: Interstadials 1 to 12. *I*, *II*: contourite peaks from Faugères et al. (1986).

CADKS24 (Fig. 2) and with very similar ages in other cores (Figs. 2 to 5).

The Bølling-Allerød (B-A) period can also be characterized by the presence of these species, but they rarely occur all together or are scarce. *T. sacculifer* is most commonly observed during the B-A.

5.2.2. Coiling direction of the species Globorotalia hirsuta

Monitoring of the coiling direction of the subtropical species *Gr. hirsuta* has been previously used to evidence the Holocene-Pleistocene stratigraphical boundary off the Moroccan and Portuguese coasts, and in the Bay of Biscay (*e.g.*, Thiede, 1971; Pujol, 1975; Sierro et al., 1999; Duprat and Cortijo, 2004). These authors and our results (Figs. 2 to 5) globally show that *Gr. hirsuta* is sinistrally coiled (90 to 100%) during the very end of the Pleistocene and gradually passes to preferentially dextral forms during the Holocene. This species becomes preferentially dextral (> 50%) between the two peaks of *Gr. truncatulinoides* TE3 and TE2 described in the following paragraph, similar to the date of 5 kyr proposed by Duprat (1983) (Fig. 2). Nevertheless, our results, such as the previous ones, note the weakness of this biostratigraphical tool as *Gr. hirsuta* is very rare in sediments, especially at the Pleistocene-Holocene boundary. It can be quite difficult to obtain enough specimens to monitor coiling, in some cases finding a complete disappearance of the species (Figs. 3 and 5). Duprat and Cortijo (2004) proposed 9 kyr for the age of the coiling change from 90 to 100% of sinistrally coiled forms to the coexistence of both dextral and sinistral forms in the Bay of Biscay. From cores presented in Fig. 2, we could propose ~10 kyr for this coiling change but the fragmentary records (Figs. 3 to 5) could also suggest diachronism between core locations in the Cádiz region and in

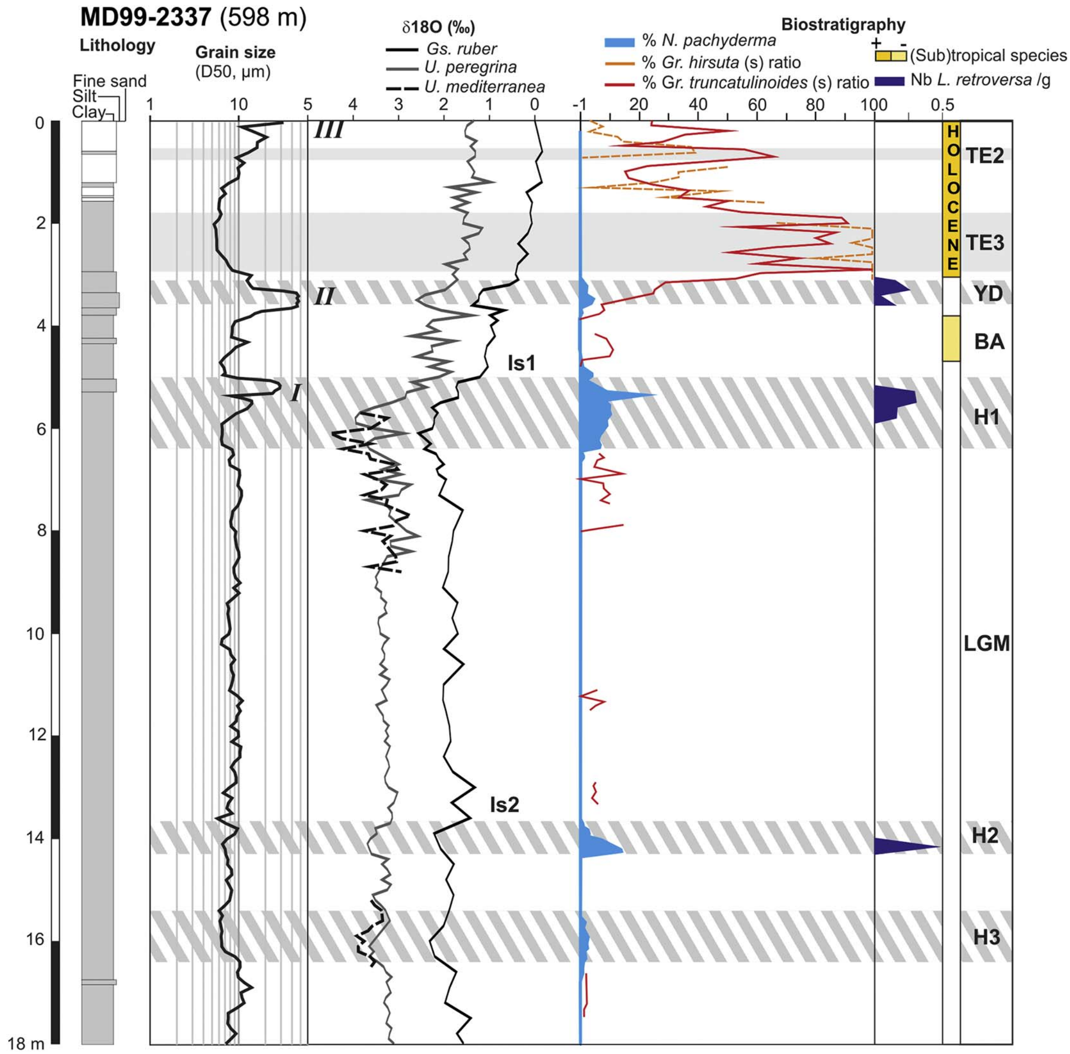

Fig. 4. Stratigraphical synthesis of the core MD99–2337, located under the MUW influence. From left to right: core log (grey: < 30% $CaCO_3$; white: > 30% $CaCO_3$), grain-size data, $\delta^{18}O$ planktonic and benthic curves, biostratigraphical curves of planktonic foraminifera and pteropods, and radiocarbon datings. TE2 to TE5: *Gr. truncatulinoides* (s) events, YD: Younger Dryas, BA: Bølling-Allerød, H1 to H3: Heinrich Stadials; LGM: Last Glacial Maximum. Is1 and Is2: Interstadials 1 and 2. *I*, *II*, *III*: contourite peaks from Faugères et al. (1986).

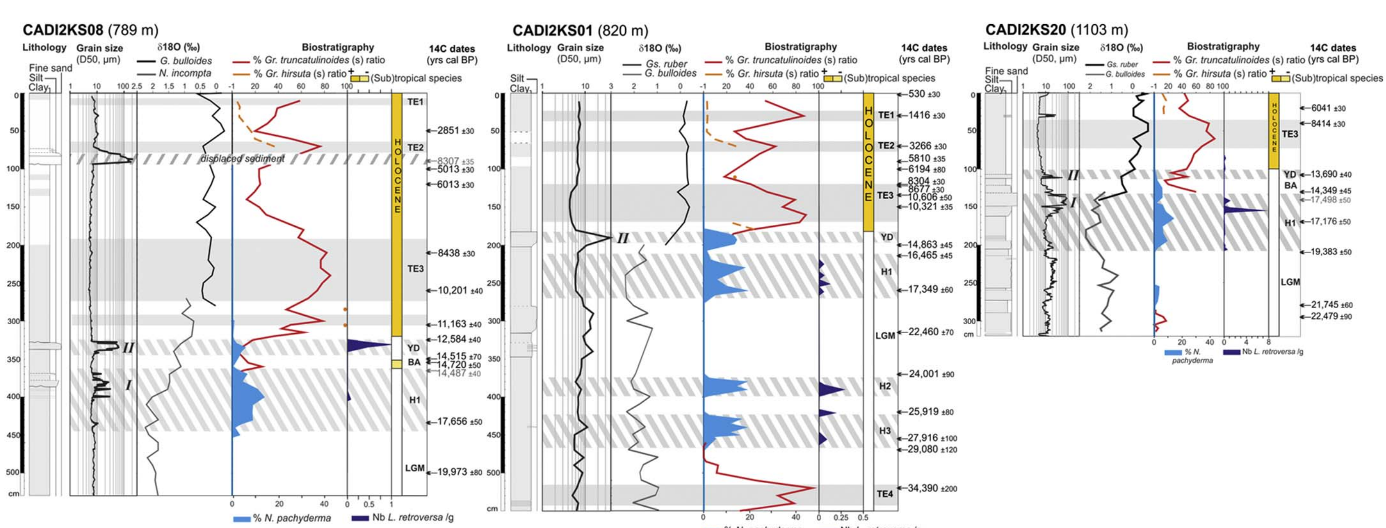

Fig. 5. Stratigraphical synthesis of the cores CADI2KS08, located under the Intermediate Branch (MLW) influence, CADI2KS01, located under the Principal Branch (MLW) influence and CADI2KS20, located under the Southern Branch (MLW) influence. From left to right: core log (grey: < 30% $CaCO_3$; white: > 30% $CaCO_3$), grain-size data, $\delta^{18}O$ composite planktonic curve, biostratigraphical curves of planktonic foraminifera and pteropods, and radiocarbon datings. TE1 to TE3: *Gr. truncatulinoides* (s) events, YD: Younger Dryas, BA: Bølling-Allerød, H1: Heinrich Stadial 1; LGM: Last Glacial Maximum. *I*, *II*: contourite peaks from Faugères et al. (1986).

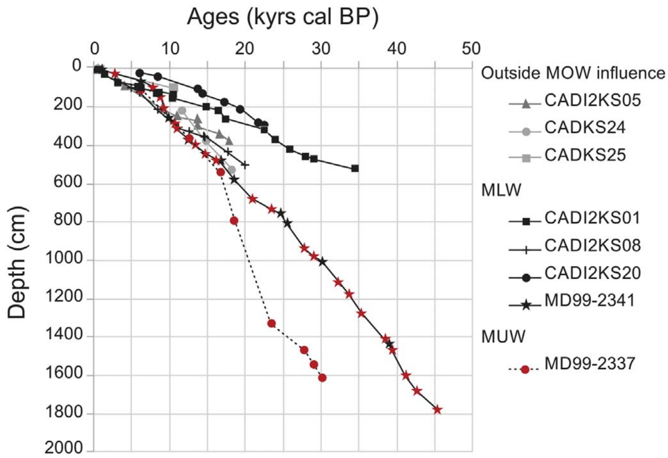

Fig. 6. Age models for reference cores over the past 50 kyr. The age model is based on ^{14}C-AMS datings (black or grey symbols) and correlation with the δ^{18}O planktonic record of core MD99-2339 (Voelker et al., 2006; tie-points are indicated with red symbols). Tie-points for the core MD99-2337 are indicated in Table 3 and for the core MD99-2341 they are presented in Toucanne et al. (2007). (For interpretation of the references to colour in this figure legend, the reader is referred to the web version of this article.)

Table 3
List of the tie-points used to construct the MD99-2337 age model thanks to a stratigraphical correlation between the planktonic δ^{18}O records of cores MD99-2337 and MD99-2339 (Gulf of Cádiz; Voelker et al., 2006).

Depth (cm)	Age (calendar kyr BP)
110	6263
365	12,643
540	16,701
790	18,585
1330	23,405
1470	27,832
1540	29,011
1610	30,112

the Bay of Biscay. Because of the scarcity of continuous records of this species in our study and the large uncertainty of coiling change identification due to the abundances of specimens being too low, we will not discuss the age of this bio-event hereafter.

5.2.3. Coiling direction of the species *Globorotalia truncatulinoides*

Coiling direction changes in *Gr. truncatulinoides* have previously been shown to be of value for the correlation between late Pleistocene cores (Ericson and Wollin, 1968). Peaks formed by increases in the percentage of sinistral forms correlate rather closely between cores and support correlations based on frequency distributions. Differences in the shapes of peaks are mainly due to changes in sedimentation rates between cores (plateau-like shape with sedimentation rates ≥ 10 cm/ka).

The first high percentages of the sinistral ratio of *Gr. truncatulinoides* observed in the sedimentary sequences of the Gulf of Cádiz, named TE1 in Figs. 2 and 5, range between 60 and 80% and occur between 700 and 1400 cal yr BP (Fig. 7; Table 4). This is observed in all cores at which Late Holocene sediments have been recovered, attesting to its regional significance.

The second peak of the *Gr. truncatulinoides* sinistral ratio, named TE2 in Figs. 2, 4 and 5, ranges from 60 to 75% and occurs between 3250 and 4250 cal yr BP (Fig. 7; Table 4). It is at the boundary between mid and late Holocene. This peak is also observed in all cores at which mid-Holocene sediments have been recovered.

The third peak is the most conspicuous one of the Holocene period. Named TE3, its *Gr. truncatulinoides* sinistral ratio exceeds 80% of and ranges from 8200 to 10,600 cal yr BP (Fig. 7; Table 4). It is observed in all cores of this study and allows easy identification of the Early Holocene.

Fine-grained sediments are observed in the different cores during those Holocene peaks of the *Gr. truncatulinoides* sinistral ratio.

The fourth peak of the *Gr. truncatulinoides* sinistral ratio, named TE4 in Figs. 3 and 5, exceeds 90% and ranges from 33,800 and 35,600 cal yr BP (Marine Isotopic Stage 3, MIS3, Interstadial 7; Fig. 7; Table 4). It is observed in all cores reaching those ages. It is characterized by fine-grained sediment in core CADI2KS01 (Bartolome Dias Drift/PB; Fig. 5) and in core MD99-2341 (Faro-Cádiz Drift/MUW; Fig. 3).

The fifth peak of the *Gr. truncatulinoides* sinistral ratio, named TE5 in Fig. 3, exceeds 80% and is older than ~43,000 cal yr BP and younger than 46,000 cal yr BP (MIS3, Interstadials 10 and 11). Fine-grained sediments are observed during this bio-event in core MD99-2341 (Faro-Cádiz Drift/MUW; Fig. 3).

5.2.4. *N. pachyderma* distribution

At least five occurrences of this polar species have been observed in the cores of the Gulf of Cádiz over the last 50 kyr.

The first occurrence of *N. pachyderma* from the tops of cores ranges from 2 to 5%, between 11,070 and 13,800 cal yr BP (Fig. 8; Table 4). This event has been previously correlated with the Younger Dryas by Rogerson et al. (2005), Llave et al. (2006), Voelker et al. (2006), Eynaud et al. (2009) and Chabaud et al. (2014). It is coeval with the most significant coarse-grained contouritic bed of the past 50 kyr in the Gulf of Cádiz, widespread in the contouritic environments: at the limit of influence of the Southern MLW Branch (Fig. 2), in the Faro-Cádiz Drift/MUW (Fig. 3), in the Faro Drift/MUW (Fig. 4) and in the Albufeira Drift/IB (Fig. 5) centred at ~12,600 cal yr BP. It is missing in the core CADI2KS05 which is the deepest core of this study and located out of the MOW influence even during the deepening of the MOW (Fig. 2).

The second occurrence of *N. pachyderma* ranges from 10 to 15% and is dated between 15,400 and 17,950 cal yr BP (Fig. 8; Table 4). It is correlated to Heinrich Stadial 1 (Turon et al., 2003; Llave et al., 2006; Voelker et al., 2006; Eynaud et al., 2009; Sanchez-Goñi and Harrison, 2010). This period is characterized by a coarser contouritic bed in all drifts and at the limit of the MOW influence at ~16,800 cal yr BP (Figs. 2 to 5) and fine-grained sediments out of the MOW influence (Fig. 2).

The third occurrence of *N. pachyderma* ranges from 10 to 12% and is dated between 23,800 and 25,500 cal yr BP (Fig. 8; Table 4). It is correlated with Heinrich Stadial 2 (Turon et al., 2003; Llave et al., 2006; Voelker et al., 2006; Sanchez-Goñi and Harrison, 2010). This bed is not really evidenced in grain-size data except for a coarser contouritic bed in core MD99-2341 at ~25,000 cal yr BP (Faro-Cádiz Drift/MUW; Fig. 3).

The fourth occurrence of *N. pachyderma* ranges from 3 to 14% and is dated between 28,000 and 30,300 cal yr BP (Fig. 8; Table 4). It is correlated with Heinrich Stadial 3 (Llave et al., 2006). This bed is not really evidenced in grain-size data.

The fifth occurrence of *N. pachyderma* ranges from 10 to 25% and is dated between 36,500 and 37,500 cal yr BP (Fig. 8; Table 4). It is correlated with Heinrich Stadial 4 (Llave et al., 2006; Eynaud et al., 2009; Sanchez-Goñi and Harrison, 2010). This event is only observed in core MD99-2341 (Faro-Cádiz Drift/MUW; Fig. 3) and corresponds to a slightly coarser-grained contouritic bed at ~37,500 cal yr BP.

5.2.5. Pteropod distribution

The general distribution of pteropods, and especially the subpolar species *Limacina retroversa*, is also of value in intercore correlation even if they are not common. Their large size (usually > 500 µm) makes them notable and easy to observe in samples.

L. retroversa is observed during or sometimes slightly preceding *N. pachyderma* peaks except for Heinrich Stadials 3 and 4, where *L. retroversa* was not observed in the Gulf of Cádiz.

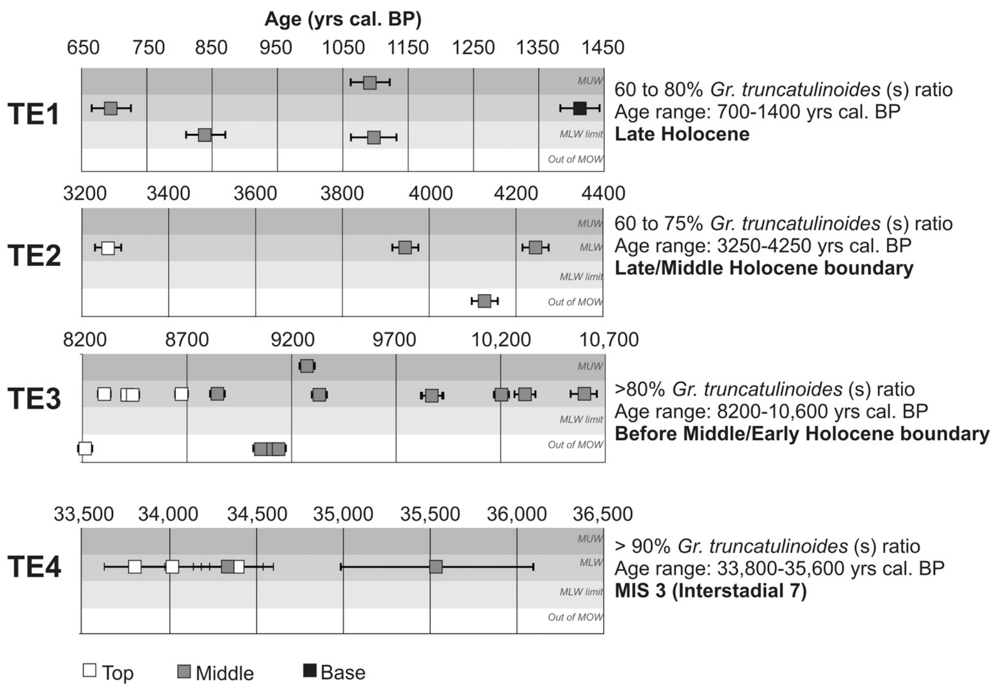

Fig. 7. Age distribution (with standard error) of proposed new biostratigraphical events (TE1 to TE4) based on radiocarbon dates from this study (Tables 2a and 2b).

During the Younger Dryas, their abundances range from 0.25 to 1 *L. retroversa*/g of sediment in almost all contouritic environments under the MOW influence or at its limit (Figs. 2 to 5). Only at the cores under the influence of the PB and SB of the MOW is *L. retroversa* absent (Bartolome Dias Drift and Portimão High, respectively; Fig. 5). At the core outside of MOW influence, *L. retroversa* occurs with 0.05 specimens/g (Fig. 2).

During Heinrich Stadial 1, *L. retroversa* abundances are almost the same in environments under and out of the MOW influence, ranging from 0.15 to 7 *L. retroversa*/g of sediment (Figs. 2 to 5).

During Heinrich Stadial 2, abundances of this species decrease to ~0.5 *L. retroversa*/g of sediment in contouritic drift environments (Figs. 3 to 5), and it is not observed in cores at the limit and out of MOW influence (Fig. 2).

6. Discussion: detailed biostratigraphy in the Gulf of Cádiz during the late Quaternary

6.1. Age of bio-events

The ages of known bio-events such as *N. pachyderma* occurrences during the Younger Dryas and Heinrich Stadials from local studies have been added to our radiocarbon date dataset for comparison (Fig. 8). The ages for Heinrich Stadials 1 to 3 are in the same range as those from the literature.

Radiocarbon dates from this study and those based on *N. pachyderma* records indicate that the Younger Dryas period is longer than expected. Specifically, the top of the event is up to ~800 years younger and the base ~700 years older than dates from local and global studies (Table 4). However, *N. pachyderma*, which are observed beyond the $\delta^{18}O$ depletions tracking this climatic event, exhibit low percentages near the noise level. Bioturbations could easily alter the signal in this sandy contourite deposit associated with this cold climatic event (Löwemark and Werner, 2001; Löwemark et al., 2004; Fig. 5) but it would also disturb the $\delta^{18}O$ signal which is not always the case (Fig. 4). The main problem in using stratigraphical tools based on continuous records such as biostratigraphy and oxygen isotope curves in this particular period is the highly reduced sediment accumulation. The Younger Dryas interval is reported as a sand-rich layer and a condensed section throughout the Gulf of Cádiz (Sierro et al., 1999; Mulder et al., 2002; Voelker et al., 2006). Our results are consistent with these observations, and sedimentation rates in the data set presented in this study are two to three times lower than in the preceding and following intervals. Tailing low abundances of *N. pachyderma* would therefore not provide a reliable identification of strictly this event, which could introduce an average age error of ± 500 yrs. However, in cores with a sufficient sediment accumulation, $\delta^{18}O$ records show the typical depletion, allowing the identification of the Younger Dryas interval, without reworking evidence despite some samples that were collected in the sand-rich contourite bed related to this climatic event (Figs. 3 and 4).

For Heinrich Stadial 4, the record is more difficult to interpret as the age error can be larger in old sediments and calibration could have changed at the H4 age range (updated calibration data sets; see Calib web site). In addition, only two radiocarbon dates are available in this study (Fig. 8; Tables 4 and 5). At least 2000 years' difference with the date usually published in the literature is observed for this same event (Sanchez-Goñi et al., 2000; Schönfeld et al., 2003; Llave et al., 2006; Voelker et al., 2006; Sanchez-Goñi and Harrison, 2010). This age offset can be related to some extent to bioturbation; infauna could transport younger sediments to a location deeper in the core, but again, as explained for the Younger Dryas interval, the associated $\delta^{18}O$ record seems to be consistent with other records that have been less affected by bioturbation than the contourite beds (Fig. 3; Voelker et al., 2006; Toucanne et al., 2007). The biostratigraphical record of *N. pachyderma* also seems consistent with the $\delta^{18}O$ curve (Fig. 3). In such a case, the age discrepancy would be preferentially related to radiocarbon age calibration. However, the only two ^{14}C datings available are not enough to prove this proposition. In a general way, in cores under the influence of an MOW branch, *N. pachyderma* abundances extend beyond the limits of the contourite beds, especially at the beginning of cold events. *N. pachyderma* occurrence and grain-size increase are almost synchronous except for the maxima of grain size and *N. pachyderma* abundances. The highest distributions of *N. pachyderma*, which translate the surface conditions, generally predate the coarsest layers related to bottom current winnowing by ~300–400 years. Bioturbation could be responsible for such an offset despite *N. pachyderma* being present in the sand fraction, but this pattern is almost always the same in the

Table 4
Radiocarbon ages of biostratigraphical events in each core.

Environment	Core	TE1	TE2	TE3	YD	H1	H2	H3	TE4	H4
MUW	CADI2K-S13	1094 ± 30[d, 2]								
	CADI2K-S11			9276 ± 40[b, 2]	11,188 ± 40[c, 1]					
MLW	MD99-2341			9868 ± 50[a, 2]	12,643 ± 50[a, 2]	17,780 ± 110[a, 3]	24,731 ± 130[a, 2]	30,112 ± 240[a, 2]	35,541 ± 560[a, 2]	37,008 ± 570[a, 1]
	CADI2K-S08			8438 ± 35[b, 1], 10,201 ± 40[b, 2]	12,584 ± 40[b, 2]	17,656 ± 50[b, 2]				
	CADI2K-S07	696 ± 30[a, 2]	3945 ± 30[b, c, 2]	8843 ± 35[d, 2]	11,170 ± 40[a, 1]					
	CADI2K-S01	1416 ± 30[a, 3]	3266 ± 30[c, 1]	8304 ± 30[a, 1], 8677 ± 30[a, 2] 10,606 ± 50[b, 2], 10,321 ± 35[c, 2]		16,465 ± 45[a, 1], 17,349 ± 60[b, 2]	24,001 ± 90[b, 2]	27,916 ± 100[d, 2] 29,080 ± 120[d, 3]	34,390 ± 200[b, 2]	
	CADI2K-S14		4244 ± 30[b, 2]		13,781 ± 50[b, 3]					
	CADI2K-S19								34,019 ± 210[e, 2]	36,869 ± 290[e, 2]
	CADI2K-S20			8414 ± 30[c, 1]	13,690 ± 40[c, 3]	17,176 ± 50[d, 2], 17,498 ± 50[d, 2]				
	CADKS09			9337 ± 40[c, 2]						
	CADKS07				12,826 ± 50[b, 2]					
	CADKS17				11,881 ± 45[c, 1]					
	CADKS04				11,450 ± 45[b, 1]	17,440 ± 80[d, 2]			33,802 ± 170[b, 2]	
	CADKS23								34,337 ± 210[b, 2]	
MOW limit	CADI2K-S17	1099 ± 35[b, 2]								
	CADKS24				11,657 ± 70[c, 1]	14,796 ± 60[b, 1], 18,256 ± 70[c, 3]				
	CADKS25	841 ± 30[b, 2]								
MOW out	CADI2K-S05		4127 ± 30[a, 2]	9088 ± 40[c, 2]	11,056 ± 35[a, 1], 13,717 ± 60[a, 3]	16,619 ± 45[a, 2], 17,943 ± 50[a, 3]				

(continued on next page)

Table 4 (*continued*)

Environment	Core	TE1	TE2	TE3	YD	H1	H2	H3	TE4	H4
	CADI2K-S22			8220 ± 45[b,1]						
	CADI2K-S23			9048 ± 40[a,2]						
	CADI2K-S24			9134 ± 30[b,2]	11,085 ± 30[b,1], 12,301 ± 35[b,2], 13,122 ± 35[b,2], 13,509 ± 40[b,3]	15,391 ± 40[b,1], 16,671 ± 50[a,2], 17,959 ± 45[a,3]				

MOW: Mediterranean Outflow Water.
MUW: Mediterranean Upper Water.
MLW: Mediterranean Lower Water.
[a] Bulk.
[b] *G. inflata.*
[c] *G. ruber alba.*
[d] *G. bulloides.*
[e] *N. incompta.*
[1] Top.
[2] Middle.
[3] Base.

twenty-two cores of this study and is also observed in cores where bioturbation is not well developed (Fig. 2). This time lag could be related to internal mechanisms between the Mediterranean and the North Atlantic climatic systems (Sierro et al., 2005; Voelker et al., 2006).

For the *Gr. truncatulinoides* sinistral ratio peaks, there is no reference at this time other than the five radiocarbon dates which constrain TE1 between 700 and 1400 cal yr BP (Fig. 8; Tables 4 and 5). This bio-event would last ~700 years and is a good marker to easily identify the Late Holocene and more particularly the European Mediaeval Warm Period (Grove and Switsur, 1994; Bianchi and McCave, 1999; Abrantes et al., 2005; Lebreiro et al., 2006). TE1 is coeval with abundant *G. hirsuta* and preferentially dextrally coiled forms (90–100%).

TE2 is only constrained by four radiocarbon dates between 3250 and 4250 cal yr BP (Fig. 7; Tables 4 and 5). This ~1000 years bio-event can be used to mark the mid Holocene and the boundary between mid and Late Holocene where isotopic data does not show great changes. *G. hirsuta* associated with this bio-event are both dextrally and sinistrally coiled (~40–50%).

TE3 is dated based on fifteen radiocarbon dates between 8200 and 10,600 cal yr BP (Fig. 7; Tables 4 and 5). It is the most obvious bio-event in the area, as this species is abundant and the peak has a plateau-like shape. When sedimentation rates are high enough, we can observe a typical two-peak shape (Figs. 2 and 5). This conspicuous bio-event lasted ~2400 years and is a good marker of the Early Holocene just under the boundary between the mid and Early Holocene. It is also coeval with the largest part of the sapropel 1 identified in Mediterranean basins (~10,500–6000 cal yr BP; *e.g.*, De Lange et al., 2008; Weldeab et al., 2014; Rohling et al., 2015). *G. hirsuta* are scarce, and the sinistrally coiled form dominates (~60%).

TE4 is only constrained by five radiocarbon dates, but they seem consistent with the stratigraphic frame. This bio-event, ranging from ~33,800 to 35,600 cal yr BP, lasted ~1800 years (Fig. 7; Tables 4 and 5). It is a significant marker of late MIS3 (Interstadial 7) as it is the last time that *Gr. truncatulinoides* sinitral is observed in this area before Termination I.

TE5 is at the limit of radiocarbon dating but seems to occur between ~44,000 and 46,000 yr BP from isotopic data, during Daansgard-Oeschger Interstadials 10 and 11 (Fig. 3). As it precedes Heinrich Stadial 4, TE5 can be a good marker associated with TE4 to identify Heinrich Stadial 4 and to place ages in MIS3, which is not always easy to constrain with only isotopic data when sedimentation rates are low.

6.2. Regional validity

The large dataset of cores used in this study was dedicated to discriminate a potential effect of reworking of microfauna and especially planktonic foraminifers and pteropods in environments under the influence of a high-velocity bottom current compared to quieter environments.

Data shown in this study do not evidence any obvious reworking or displacement of planktonic foraminifers and pteropods as the frequencies, percentages and ages of the bio-events are all coherent. We particularly do not observe any old planktonic specimens or inconsistent isotopic records in contouritic drifts where bottom currents could have reworked or displaced older microfossils (Table 3). Reworking of planktonic tests would be very reduced and microfossils would settle in a time period that is included in the different errors induced by sampling and sedimentation rates, bioturbations, species used for AMS radiocarbon measurements and standard errors. Comparisons of dates measured on different planktonic species do not show discrepancies, even between surficial species and bulk, including deep-dwelling taxa.

The *G. hirsuta* coiling change and *L. retroversa* records are subject to caution as the specimen number in samples is often too low to build a consistent pattern alone. Except for these two species with low abundances, we do not observe any local effect or diachronism in the

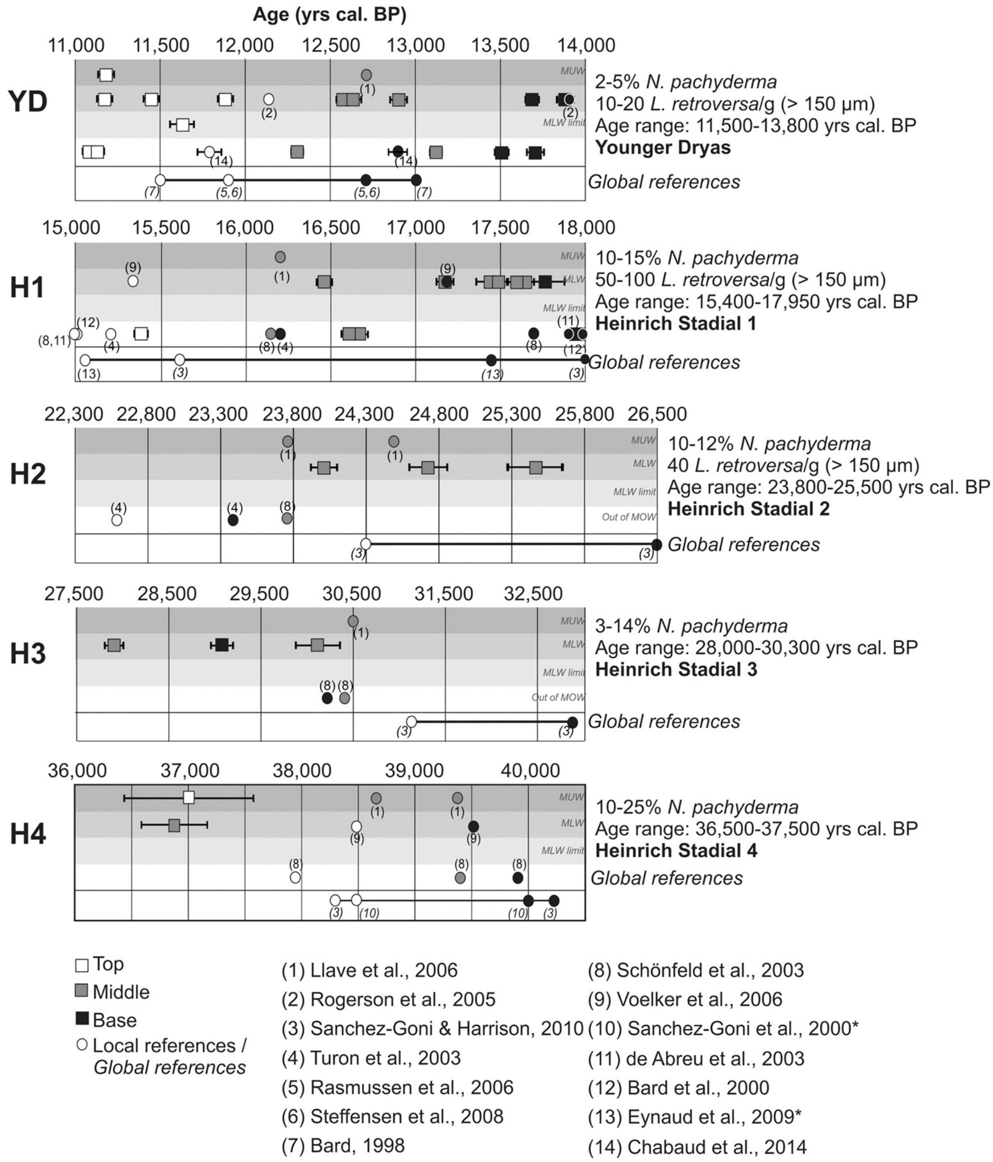

Fig. 8. Age distribution (with standard error when known) of known biostratigraphical events (YD and H1 to H4) with radiocarbon dates from this study (Tables 2a and 2b) and from the literature. Ages indicated for samples of this study correspond to the presence of *N. pachyderma*. * ^{14}C in Elliot et al. (1998, 2001).

described bio-events: all bio-events presented in this study have a very coherent signal in all of the Gulf of Cádiz. That is encouraging for detailed comparison between cores from different drifts and environments to determine, for example, which branch of the MOW was the most active during certain periods or to evaluate in detail the sedimentation rates in environments where radiocarbon dates are not always attainable because of their high terrigenous content of sediment and low presence of microfossils.

It is interesting to note that *N. pachyderma* percentages are generally higher during Heinrich Stadials 1 and 4 than during Heinrich Stadials 2 and 3 in the Gulf of Cádiz, except in the northernmost drifts (*e.g.*, core CADI2KS01 in Fig. 5). The results of Mulder et al. (2002) and Colmenero-Hidalgo et al. (2004) show decreases in $\delta^{18}O$ during Heinrich Stadials 1 and 4 but not during Heinrich Stadials 2 and 3 in the Gulf of Cádiz. This observation can be correlated with the conclusions of Cacho et al. (1999) and Sierro et al. (2005), who described prominent

Table 5
Age ranges of proposed and known biostratigraphical events and characterization. GTS: ration of *Gr. truncatulinoides* sinistral.

Bio-event	Character	Age range (years cal. BP)	Identification
TE1	60– > 80% GTS	700–1400	Late Holocene/Medieval Warm Period
TE2	60–75% GTS	3250–4250	Limit Late/Mid Holocene
TE3	> 80% GTS	8200–10,600	Early Holocene
YD	2–5% *N. pachyderma*	11,500–13,800	Younger Dryas
H1	10–15% *N. pachyderma*	15,350–17,950	Heinrich Stadial 1
H2	10–12% *N. pachyderma*	23,800–24,500	Heinrich Stadial 2
H3	3–14% *N. pachyderma*	28,000– > 30,200	Heinrich Stadial 3
TE4	> 90% GTS	33,800–35,600	MIS3/Interstadial 7
H4	10–25% *N. pachyderma*	36,500– > 37,500	Heinrich Stadial 4
TE5	> 80% GTS	> 44,164	MIS3/Interstadials 10–11

^{18}O depletions during all Heinrich Stadials in the Alboran Sea (Mediterranean side of the strait of Gibraltar) and the Menorca area (northwestern Mediterranean). These authors propose to explain this contradiction by a northern route followed by the icebergs or iceberg-derived freshwater in the Gulf of Cádiz during Heinrich Stadials 2 and 3. This proposition is confirmed with our results, at least for Heinrich Stadial 2.

Gr. hirsuta and *Gr. truncatulinoides* coiling changes have been previously described in the Cádiz region and in the Bay of Biscay (*e.g.*, Pujol, 1975; Duprat, 1983; Sierro et al., 1999). We already explained that the low abundances of *Gr. hirsuta* close to the Pleistocene-Holocene boundary cause difficulties in the use of this species as a robust stratigraphic marker. Moreover, the age of coiling change could be diachronous between the Bay of Biscay (9 kyr BP proposed by Duprat and Cortijo, 2004) and the Gulf of Cádiz (~10 kyr cal BP). The conspicuous TE3 bio-event is well identified in cores from the Bay of Biscay, the Iberian margin and the Rockall Trough with ages (6–10 kyr cal BP) consistent with those presented in this study (Pujol, 1975; Duprat, 1983; Rossignol et al., 2016), demonstrating that the interest in this bio-event is larger than regional. However, such bio-events related to *Gr. truncatulinoides* have not been observed in the western part of the North Atlantic (*e.g.*, Ericson and Wollin, 1968; Chabaud, 2016) or in the Mediterranean basins (*e.g.*, Duprat, 1983; Ducassou et al., 2007; Angue Minto'o, 2014).

6.3. Meaning of high percentages of Gr. truncatulinoides sinistral

This species, whatever the coiling direction, is present over the last 50 ka except during the coldest periods or phases. *Gr. truncatulinoides* dextral is accustomed to living between 250 and 400 m water depth, below the mixed layer (Wilke et al., 2009; Mulitza et al., 1997; Ganssen and Kroon, 2000) and the winter thermocline (Wilke et al., 2009), and it is associated with the Eastern North Atlantic Central Water (ENACW; Voelker et al., 2009). The high percentages of the sinistral form of *Gr. truncatulinoides* would suggest a deepening of living depth of this species as the sinistral forms were formerly observed in deeper water masses than the dextral forms in previous studies (Lohmann and Schweitzer, 1990; Ujiié et al., 2010).

We have no data of living *Gr. truncatulinoides* sinistral in the Gulf of Cádiz and no indication of their optimal living water depth, but we can assume that if the dextral form lives in ENACW (presently ~100 to 300–600 m, depending on location), the sinistral form could live at the transition between ENACW and MOW (presently 300 to 600 m, depending on the MOW branch and location).

Such living depths and water mass transitions are coherent with those observed in other locations in the Atlantic Ocean (Ujiié et al., 2010) and correspond to periods when MOW is in a shallow position as MOW tends to deepen during cold periods and phases such as YD or Heinrich events (Schönfeld and Zahn, 2000; Mulder et al., 2002; Rogerson et al., 2005; Voelker et al., 2006; Toucanne et al., 2007). High percentages of the sinistral ratio of *Gr. truncatulinoides* are effectively interbedded between coarser beds related to increased and deepened MOW. The fine-grained sediments that characterize these periods of *G. truncatulinoides* sinistral abundance can be related to weak MOW intensity or MOW core migration. As the different cores presented in this study are spatially widely separated under the different MOW branches and at various depths, it is more likely that MOW intensity was reduced (less winnowing) during these TE periods. During the Early Holocene, TE3 is coeval with the sapropel 1 deposition in the Mediterranean basins (6–10 kyr cal BP), characterized with a greatly reduced outflow of Mediterranean water (Rogerson et al., 2005). This period is strongly implied by the complete absence of sandy contourite from the Gulf of Cádiz slope, between peak contourites II and III (Figs. 3 to 5; Faugères et al., 1984, 1986; Nelson et al., 1993). Those TE could then be referred to the migration of MOW in its upper location with the most conspicuous TE3 related to the sapropel 1 deposition in the Mediterranean.

Rohling et al. (1995) described in their foraminiferal record from the Alboran Sea a deepening of the pycnocline position at ~8000 yr BP. These authors propose this deeper pycnocline to be related to sea level rise since the last glacial maximum. This could be coherent again with the end of TE3 in the Gulf of Cádiz at ~8200 cal yr BP and relative high sea-levels are conditions required for shallower MOW locations.

Higher sea levels during MIS 3 relative to LGM may underlie the repeated observations. Interstadials 10 and 11 are characterized by the highest sea levels during MIS 3 until 50 kyr (−60 to −40 m depending on authors; *e.g.*, Siddall et al., 2008), and this could again have favoured conditions required for shallower MOW locations.

Gr. truncatulinoides sinistrally coiled events are described along the MOW pathway: in the Gulf of Cádiz (this study), along the western Iberian margins, in the Bay of Biscay and to the Rockall Trough (Pujol, 1975; Duprat, 1983; Rossignol et al., 2016), but they have not been observed in the Mediterranean (*i.e.*, Alboran Sea; Duprat, 1983) or in the northwestern Atlantic (*e.g.*, Ericson and Wollin, 1968; Chabaud, 2016). More comparisons with the frequencies of both forms of this species from other regions of North Atlantic and isotope analyses of tests are required, but the presented data suggest that their presence is closely related to northeastern Atlantic water mass structure and dynamics. The most conspicuous event TE3, probably related to sapropel 1 deposition, is observed in all the cores of the Gulf of Cádiz but also along the Portuguese margins and in the Bay of Biscay. The cores of the Gulf of Cádiz presented in this study are all located under the MOW plume but we can observe higher ratios of sinistrally coiled *Gr. truncatulinoides* (80 to 100%) in cores located directly under the MOW main pathway (Figs. 1 and 3 to 5) than in cores located in the central part of the Gulf of Cádiz (60 to 80%; Figs. 1 and 2). This ratio also ranges from 60 to 80% for TE3 along the Portuguese margins and in the Bay of Biscay (Rossignol et al., 2016), which could mimic proximal/outlying and proximal/distal distributions.

7. Conclusions

The two objectives of this paper were (1) to propose a biostratigraphic framework of the last 50 ka in the Gulf of Cádiz with a robust age control based on a large radiocarbon and oxygen isotope data set, and (2) to test the reliability of faunal-based analyses in a bottom current-dominated environment characterized by high-velocity currents.

Biostratigraphical events of the Holocene and Late Pleistocene ages from the Gulf of Cádiz and based on planktonic foraminifera and pteropods show a high degree of similarity regardless of sedimentation rates and sedimentary environments. A detailed correlation between cores of contouritic drifts and slope environments without high-velocity bottom current influence is achieved through coiling direction changes within *Globorotalia truncatulinoides* and *Globorotalia hirsuta*, and by occurrences of the polar species *Neogloboquadrina pachyderma* and *Limacina retroversa*. The latter two species are related to paleoclimatic oscillations and illustrate the last six rapid changing water-mass conditions at the surface of the Gulf of Cádiz over the past 50 ka (Heinrich Stadials and Younger Dryas). The *Globorotalia hirsuta* coiling change could be a good indicator for locating the Pleistocene-Holocene boundary in the region but the very low abundances of this species at this boundary make it difficult to apply. *Globorotalia truncatulinoides* sinistral events may reflect MOW migration and especially with five periods with its shallowest vertical location over the last 50 ka (Holocene and MIS3). These surface-to-subsurface biostratigraphical markers are fully suitable to regional comparisons between areas under and outside of high-velocity bottom currents. They could be especially suited to compare the spatial behaviour of the different branches of the MOW with a high resolution.

Acknowledgements

The authors thank the crew and scientific teams of CADISAR 1 and 2 cruises on the r/v *Le Suroît* and GINNA/IMAGES V cruise on the r/v *Marion Dufresne II* (IPEV) for the recovery of the cores, and J. Saint-Paul and G. Chabaud for their invaluable technical assistance. We also thank A.H.L. Voelker and an anonymous reviewer whose comments further improved this paper. Finally, the authors thank the French programmes Action Marges for financial support and Artémis for most of the radiocarbon dating of this study.

Appendix A. Supplementary data

Supplementary data to this article can be found online at https://doi.org/10.1016/j.margeo.2017.09.014.

References

Abrantes, F., Lebreiro, S., Rodrigues, T., Gil, I., Bartels-Jonsdottir, H.B., Oliveira, P., Kissel, C., Grimalt, J.O., 2005. Shallow-marine sediment cores record climate variability and earthquake activity off Lisbon (Portugal) for the last 2000 years. Quat. Sci. Rev. 24, 2477–2494.

Ambar, I., Howe, M.R., 1979. Observations of the Mediterranean Outflow - II. The deep circulation in the vicinity of the Gulf of Cadiz. Deep Sea Res. Part A 26, 555–568.

Ambar, I., Armi, L., Bower, A., Ferreira, T., 1999. Some aspects of time variability of the Mediterranean Water off south Portugal. Deep-Sea Res. I Oceanogr. Res. Pap. 46 (7), 1109–1136.

Angue Minto'o, C.M., 2014. Enregistrements sédimentaires des changements climatiques et environnementaux pendant le Quaternaire terminal sur la marge est-Corse. PhD Thesis. University of Perpignan (313 pp.).

Bahr, A., Kaboth, S., Jiménez-Espejo, F.J., Sierro, F.J., Voelker, A.H.L., Lourens, L., Röhl, U., Reichart, G.J., Escutia, C., Hernandez-Molina, F.J., Friedrich, O., 2015. Persistent monsoonal forcing of Mediterranean Outflow Water dynamics during the late Pleistocene. Geology G37013.

Bé, A.W.H., 1960. Ecology of recent planktonic foraminifera. Part 2 – bathymetric and seasonal distributions in the Sargasso Sea off Bermuda. Micropaleontology 6 (4), 373–392.

Bé, A.W.H., 1977. An ecological, zoogeographic and taxonomic review of recent planktonic foraminifera. In: Ramsay, A.T.S. (Ed.), Oceanic Micropaleontology. Vol. 1. Academic Press, pp. 1–100.

Bé, A.W.H., Gilmer, R.W., 1977. In: Ramsay, A.T.S. (Ed.), Oceanic Micropaleontology. Academic Press (812 pp.).

Bé, A.W.H., Tolderlund, D.S., 1971. Distribution and ecology of living planktonic foraminifera in surface waters of the Atlantic and Indian oceans. In: Funnell, B.M., Riedel, W.R. (Eds.), Micropaleontology of Marine Bottom Sediments. Cambridge University Press, Cambridge, pp. 105–149.

Bianchi, G.G., McCave, I.N., 1999. Holocene periodicity in North Atlantic climate and deep-ocean flow south of Iceland. Nature 397, 515–517.

Bolli, H.M., Saunders, J.B., Perch-Nielsen, K., 1989. Plankton Stratigraphy Volume 1: Planktic Foraminifera, Calcareous Nannofossils and Calpionellids. Cambridge University Press (608 pp.).

Boyum, G., 1967. Hydrological observations of the M/S Helland-Hansen and current measurements in the area west of Gibraltar, May 1965. In: NATO Sub-Commitee Oceanographic Research, Technical Report 34, pp. 35–36.

Bryden, H.L., Stommel, H.M., 1982. Origin of the Mediterranean outflow. J. Mar. Res. 40S, 55–71.

Cacho, I., Grimalt, J.O., Pelejero, C., Canals, M., Sierro, F.J., Flores, J.A., Shackleton, N., 1999. Dansgaard-Oeschger and Heinrich event imprints in Alboran Sea paleotemperatures. Paleoceanography 14, 698–705.

Chabaud, L., 2016. Modèle stratigraphique et processus sédimentaires au Quaternaire sur deux pentes carbonatées des Bahamas (leeward et windward). PhD Thesis. University of Bordeaux (421 pp.).

Chabaud, L., Sánchez Goñi, M.F., Desprat, S., Rossignol, L., 2014. Land-sea climatic variability in the eastern North Atlantic subtropical region over the last 14,200 years: atmospheric and oceanic processes at different timescales. The Holocene 24, 787–797.

Cléroux, C., Lynch-Stieglitz, J., Schmidt, M.W., Cortijo, E., Duplessy, J.-C., 2009. Evidence for calcification depth change of *Globorotalia truncatulinoides* between deglaciation and Holocene in the Western Atlantic Ocean. Mar. Micropaleontol. 73, 57–61.

Colmenero-Hidalgo, E., Flores, J.A., Sierro, F.J., Bárcena, M.A., Löwemark, L., Schönfeld, J., Grimalt, J.O., 2004. Ocean surface water response to short-term climate changes revealed by coccolithophores from the Gulf of Cádiz (NE Atlantic) and Alboran Sea (W Mediterranean). Palaeogeogr. Palaeoclimatol. Palaeoecol. 205, 317–336.

Darling, K.F., Kucera, M., Kroon, D., Wade, C.M., 2006. A resolution for the coiling ratio direction paradox in *Neogloboquadrina pachyderma*. Palaeoceanography 21, 2011–2034.

De Abreu, L., Shackleton, N.J., Schönfeld, J., Hall, M., Chapman, M., 2003. Millennial-scale oceanic climate variability off the western Iberian margin during the last two glacial periods. Mar. Geol. 196, 1–20.

De Lange, G.J., Thomson, J., Reitz, A., Slomp, C.P., Speranza Principato, M., Erba, E., Corselli, C., 2008. Synchronous basin-wide formation and redox-controlled preservation of a Mediterranean sapropel. Nat. Geosci. 1, 606–610.

Ducassou, E., Capotondi, L., Murat, A., Bernasconi, S.M., Mulder, T., Gonthier, E., Migeon, S., Duprat, J., Giraudeau, J., Mascle, J., 2007. Multi proxy late quaternary stratigraphy - a step toward a chronology of deep-sea terrigeneous systems - example of the Nile deep-sea turbidite system. Sediment. Geol. 200, 1–13.

Duprat, J., 1983. Les foraminifères planctoniques du Quaternaire terminal d'un domaine péricontinental (Golfe de Gascogne, côtes ouest-ibériques, Mer d'Alboran): écologie, biostratigraphie. Bull. Inst. Géol. Bassin Aquitaine 33, 71–150.

Duprat, J., Cortijo, E., 2004. *Globorotalia hirsuta*: a stratigraphic marker for the Upper Holocene in the North Atlantic Ocean. In: 8th International Conference on Paleoceanography (ICP 8), 5–10 September 2004, Biarritz, France.

Elliot, M., Labeyrie, L., Bond, G., Cortijo, E., Turon, J.-L., Tisnerat, N., Duplessy, J.C., 1998. Millenial-scale iceberg discharges in the Irminger Basin during the last glacial period: relationship with the Heinrich events and environmental settings. Paleoceanography 13, 433–446.

Elliot, M., Labeyrie, L., Dokken, T., Manthé, S., 2001. Coherent patterns of ice-rafted debris deposits in the Nordic regions during the last glacial (10–60 ka). Earth Planet. Sci. Lett. 194 (1–2), 151–163.

Ericson, D.B., Wollin, G., 1968. Pleistocene climates and chronology in deep-sea sediments. Science 13, 1227–1234.

Eynaud, F., de Abreu, L., Voelker, A.H.L., Schonfeld, J., Salgueiro, E., Turon, J.-L., Penaud, A., Toucanne, S., Naughton, F., Sanchez-Goñi, M.F., Malaizé, B., Cacho, I., 2009. Position of the Polar Front along the western Iberian margin during key cold episodes of the last 45 ka. Geochem. Geophys. Geosyst. 10, 1–21.

Faugères, J.-C., Gonthier, E., Stow, D.A.V., 1984. Contourite drift molded by deep Mediterranean outflow. Geology 12, 296–300.

Faugères, J.-C., Gonthier, E., Peypouquet, J.-P., Pujol, C., Vergnaud-Grazzini, C., 1986. Distribution et variations des courants de fond sur la ride de Faro (golfe de Cadix), témoins des modifications des échanges Méditerranée-Atlantique au Quaternaire récent. Bull. Soc. Geol. Fr. 3, 423–432.

Faugères, J.-C., Gonthier, E., Monteiro, J.H., Vergnaud-Grazzini, C., 1994. Sedimentary records of deep contour currents: an example, the Mediterranean Outflow in the late Quaternary. Comunicações Instituto Geológico e Mineiro 80, 71–88.

Ganssen, G.M., Kroon, D., 2000. The isotopic signature of planktonic foraminifera from NE Atlantic surface sediments: implications for the reconstruction of past oceanic conditions. J. Geol. Soc. 157, 693–699.

Gonthier, E., Faugères, J.-C., Stow, D.A.V., 1984. Contourite facies of the Faro drift, Gulf of Cadiz. In: Stow, D.A.V., Piper, D.J.W. (Eds.), Fine-Grained Sediments: Deep Water and Processes. Vol. 15. Geological Society by Blackwell Scientific Publications, Oxford London Edinburg, pp. 245–256.

Grove, J.M., Switsur, V.R., 1994. Glacial geological evidence for the Medieval Warm Period. Climate Change 26, 143–169.

Habgood, E.L., Kenyon, N.H., Masson, D.G., Akhmetzhanov, A., Weaver, P.P.E., Gardner, J.M., Mulder, T., 2003. Deep-water sediment wave fields, bottom current sand channels and gravity flow channel-lobe systems: gulf of Cadiz, NE Atlantic. Sedimentology 50 (3), 483–510.

Hanquiez, V., 2006. Processus sédimentaires et activité de la Veine d'Eau Méditerranéenne au cours du Quaternaire terminal dans le Golfe de Cadix. PhD thesis. Vol. 1 Université Bordeaux (352 pp.).

Hanquiez, V., Mulder, T., Lecroart, P., Gonthier, E., Marchès, E., Voisset, M., 2007. High resolution seafloor images in the Gulf of Cadiz, Iberian margin. Mar. Geol. 246, 42–59.

Heezen, B.C., Hollister, C.D., Ruddiman, W.F., 1966. Shaping of the continental rise by deep geostrophic contour currents. Science 152, 502–508.

Heinrich, H., 1988. Origin and consequences of cyclic ice rafting in the northeast Atlantic Ocean during the past 130,000 years. Quat. Res. 29, 142–152.

Hemleben, C., Spindler, M., Anderson, O.R., 1983. Modern Planktonic Foraminifera. Springer-Verlag, New York (363 pp.).

Hemleben, C., Spindler, M., Breitinger, I., Deuser, W.G., 1985. Field and laboratory studies on the ontogeny and ecology of some globorotaliid species from the Sargasso Sea off Bermuda. J. Foraminifera Reasearch 15, 254–272.

Hernández-Molina, F.J., Llave, E., Somoza, L., Fernández-Puga, M.C., Maestro, A., León, R., Medialdea, T., Barnolas, A., García, M., Dias del Río, V., Fernández-Salas, L.M., Vázquez, J.T., Lobo, F.J., Alveirinho Dias, J.M., Rodero, J., Gardner, J.M., 2003. Looking for clues to paleoceanographic imprints: a diagnosis of the Gulf of Cadiz contourite depositional systems. Geology 31 (1), 19–22.

Hernández-Molina, F.J., Llave, E., Stow, D.A.V., García, M., Somoza, L., Vázquez, J.T., Lobo, F.J., Maestro, A., Diaz del Río, V., León, R., 2006. The contourite depositional system of the Gulf of Cadiz: a sedimentary model related to the bottom current activity of the Mediterranean Outflow Water and its interaction with the continental margin. Deep-Sea Res. II Top. Stud. Oceanogr. 53 (11 – 13), 1420–1463.

Hernández-Molina, F.J., Serra, N., Stow, D.A.V., Llave, E., Ercilla, G., Van Rooij, D., 2011. Along-slope oceanographic processes and sedimentary products around the Iberian margin. Geo-Mar. Lett. 31, 315–341.

Janssen, A.W., 2006. Holoplanktonic mollusca (Gastropoda) from the Gulf of Aqaba, Red Sea and Gulf of Aden (Late Holocene-Recent). Veliger 49 (3), 140–195.

Jungclaus, J.H., Mellor, G.L., 2000. A three-dimensional model study of the Mediterranean Outflow. J. Mar. Syst. 24 (1–2), 41–66.

Kaboth, S., Bahr, A., Reichart, G.-J., Jacobs, B., Lourens, L.J., 2015. New insights into the upper MOW variability over the last 150 kyr from IODP 339 Site U1386 in the Gulf of Cádiz. Mar. Geol. 377, 136–145.

Kennett, J.P., Srinivasan, M.S., 1983. Neogene Planktonic Foraminifera: A Phylogenetic Atlas. Hutchinson Ross Publishing Company (265 pp.).

Kenyon, N.H., Belderson, R.H., 1973. Bed forms of the Mediterranean undercurrent observed with side-scan sonar. Sediment. Geol. 9 (2), 77–99.

Knutz, P.C., 2008. Chapter 24 Palaeoceanographic Significance of Contourite Drifts. In: Rebesco, M., Camerlenghi, A. (Eds.), Contourites. Developments in Sedimentology. Vol. 60. pp. 511–536.
Laberg, J.S., Vorren, T.O., Knutsen, S.M., 1999. The Lofoten contourite drift off Norway. Mar. Geol. 159, 1–6.
Lebreiro, S.M., Frances, G., Abrantes, F.F.G., Diz, P., Bartels-JOnsdottir, H.B., Stroynowski, Z.N., Gil, I.M., Pena, L.D., Rodrigues, T., Jones, P.D., Nombela, M.A., Alejo, I., Briffa, K.R., Harris, I., Grimalt, J.O., 2006. Climate changes and coastal hydrographic response along the Atlantic Iberian margin (Tagus Prodelta and Muros Ria) during the last two millennia. The Holocene 16, 1003–1015.
Llave, E., Schönfeld, J., Hernández-Molina, F.J., Mulder, T., Somoza, L., Dıaz del Río, V., Sanchez-Almazo, I., 2006. High-resolution stratigraphy of the Mediterranean outflow contourite system in the Gulf of Cadiz during the late Pleistocene: the impact of Heinrich events. Mar. Geol. 227, 241–262.
Lohmann, G.P., Schweitzer, P.N., 1990. *Globorotalia truncatulinoides* growth and chemistry as probes of the past thermocline: 1 Shell size. Paleoceanography 5 (1), 55–75.
Löwemark, L., Werner, F., 2001. Dating errors in high-resolution stratigraphy: a detailed X-ray radiograph and AMS 14C study of Zoophycus burrows. Mar. Geol. 177, 191–198.
Löwemark, L., Schoenfeld, J., Werner, F., Schaefer, P., 2004. Trace fossils as a paleoceanographic tool: evidence from Late Quaternary sediments of the southwestern Iberian margin. Mar. Geol. 204, 27–41.
Madelain, F., 1970. Influence de la topographie du fond sur l'écoulement méditerranéen entre le détroit de Gibraltar et le Cap St Vincent. Cah. Oceanogr. 22 (1), 43–61.
Marani, M., Argnani, A., Roveri, M., Trincardi, F., 1993. Sediment drifts and erosional surfaces in the central Mediterranean: seismic evidence of bottom-current activity. Sediment. Geol. 82, 207–220.
Marchès, E., Mulder, T., Cremer, M., Bonnel, C., Hanquiez, V., Gonthier, E., Lecroart, P., 2007. Contourite drift construction influenced by capture of Mediterranean Outflow Water deep-sea current by the Portimão submarine canyon (Gulf of Cadiz, South Portugal). Mar. Geol. 242, 247–260.
McCave, I.N., Manighetti, B., Robinson, S.G., 1995. Sortable silt and fine sediment size/composition slicing: parameters for palaeocurrent speed and palaeoceanography. Paleoceanography 10, 593–610.
Mulder, T., Lecroart, P., Voisset, M., Schönfeld, J., Le Drezen, E., Gonthier, E., Hanquiez, V., Zahn, R., Faugères, J.-C., Hernández-Molina, F.J., Llave-Barranco, E., Gervais, A., 2002. Past deep-ocean circulation and the paleoclimate record, Gulf of Cadiz. Eos. Trans. AGU 83 (43), 481–488.
Mulitza, S., Dürkoop, A., Hale, W., Wefer, G., Niebler, H.S., 1997. Planktonic foraminifera as recorders of past surface-water stratification. Geology 25, 335–338.
Mulitza, S., Arz, H.W., Mücke, Moos, C., Niebler, H.S., Pätzold, J., Segl, M., 1999. The South Atlantic carbon isotope record of planktic foraminifera. In: Fisher, G., Wefer, G. (Eds.), Use of Proxies in Paleoceanography: Examples from the South Atlantic. Springer, New York, pp. 427–445.
Nelson, C.H., Baraza, J., Maldonado, A., 1993. Mediterranean undercurrent sandy contourites, Gulf of Cadiz, Spain. Sediment. Geol. 82 (1–4), 103–131.
O'Neil-Baringer, M., Price, J.F., 1999. A review of the physical oceanography of the Mediterranean Outflow. Mar. Geol. 155, 63–82.
Pujol, C., 1975. Intérêt des variations du sens d'enroulement de *Globorotalia truncatulinoides* (d'Orbigny) et de *Globorotalia hirsuta* (d'Orbigny) dans la stratigraphie du Pléistocène supérieur et de l'Holocène du Golfe de Gascogne. In: Revista Española de Micropaleontologia, Madrid MCMLXXIV Numero especial, pp. 107–116.
Rebesco, M., Camerlenghi, A. (Eds.), 2008. Contourites. Vol. 60 Elsevier, Amsterdam Developments in Sedimentology. (663 pp.).
Reimer, P.J., Baillie, M.G.L., Bard, E., Bayliss, A., Beck, J.W., Blackwell, P.G., Ramsey, C.B., Buck, C.E., Burr, G.S., Edwards, R.L., Friedrich, M., Grootes, P.M., Guilderson, T.P., Hajdas, I., Heaton, T.J., Hogg, A.G., Hughen, K.A., Kaiser, K.F., Kromer, B., McCormac, F.G., Manning, S.W., Reimer, R.W., Richards, D.A., Southon, J.R., Talamo, S., Turney, C.S.M., van der Plicht, J., Weyhenmeyer, C.E., 2009. IntCal09 and Marine09 radiocarbon age calibration curves, 0–50,000 years CAL BP. Radiocarbon 51 (4), 1111–1150.
Rogerson, M., Rohling, E.J., Weaver, P.P.E., Murray, J.W., 2005. Glacial to interglacial changes in the settling depth of the Mediterranean Outflow plume. Paleoceanography 20, 1–12.
Rohling, E.J., Den Dulk, M., Pujol, C., Vergnaud-Grazzini, C., 1995. Abrupt hydrographic change in the Alboran Sea (western Mediterranean) around 8000 yrs BP. Deep-Sea Res. I Oceanogr. Res. Pap. 42, 1609–1619.
Rohling, E.J., Marino, G., Grant, K.M., 2015. Mediterranean climate and oceanography, and the periodic development of anoxic events (sapropels). Earth Sci. Rev. 143, 62–97.
Rossignol, L., Ducos, S., Aimon, C., Eynaud, F., Duprat, J., 2016. Coiling ratio of *Globorotalia truncatulinoides*: a robust stratigraphic tool in the North East-Atlantic during the Holocene. In: Foraminifera and Nannofossil Groups Joint Spring Meeting 2016, 19th–24th June. Angers, France.
Sanchez-Goñi, M.F., Harrison, S.P., 2010. Millennial-scale climate variability and vegetation changes during the last glacial: concepts and terminology. Quat. Sci. Rev. 29, 2823–2827.
Sanchez-Goñi, M.F., Turon, J.-L., Eynaud, F., Gendreau, S., 2000. European climatic response to millenial-scale changes in the atmosphere-ocean system during the Last Glacial Period. Quat. Res. 54, 394–403.
Schiebel, R., Joanna, W., Matthias, B., Hemleben, C., 2001. Planktic foraminiferal production stimulated by chlorophyll redistribution and entrainment of nutrients. Deep Sea Res., Part I 721–740.
Schönfeld, J., Zahn, R., 2000. Late Glacial to Holocene history of the Mediterranean Outflow. Evidence from benthic foraminiferal assemblages and stable isotopes at the Portuguese margin. Palaeogeogr. Palaeoclimatol. Palaeoecol. 159, 85–111.
Schönfeld, J., Zahn, R., de Abreu, L., 2003. Surface to deep water response to rapid climate changes at the western Iberian Margin. Glob. Planet. Chang. 36 (4), 237–264.
Siddall, M., Rohling, E.J., Thompson, W.G., Waelbroeck, C., 2008. Marine isotope stage 3 sea level fluctuations: data synthesis and new outlook. Rev. Geophys. 46 (RG4003). http://dx.doi.org/10.1029/2007RG000226.Sierro.
Sierro, F.J., Flores, J.A., Baraza, J., 1999. Late glacial to recent paleoenvironmental changes in the Gulf of Cadiz and formation of sandy contourite layers. Mar. Geol. 155, 157–172.
Sierro, F.J., Hodell, D.A., Curtis, J.H., Flores, J.A., Reguera, I., Comero-Hidalgo, E., Báarcena, M.A., Grimalt, J.O., Cacho, I., Frigola, J., Canals, M., 2005. Impact of iceberg melting on Mediterranean thermohaline circulation during Heinrich events. Paleoceanography 20, 1–13.
Somoza, L., Diaz-del-Rio, V., León, R., Ivanov, M., Fernández-Puga, M.C., Gardner, J.M., Hernández-Molina, F.J., Pinheiro, L.M., Rodero, J., Lobato, J., 2003. Seabed morphology and hydrocarbon seepage in the Gulf of Cadiz mud volcano area: acoustic imagery, multibeam and ultra-high resolution seismic data. Mar. Geol. 195 (1–4), 153–176.
Spezzaferri, S., Kucera, M., Pearson, P.N., Wade, B.S., Rappo, S., Poole, C.R., Morard, R., Stalder, C., 2015. Fossil and genetic evidence for the polyphyletic nature of the planktonic foraminifera "*Globerinoides*", and description of the new genus *Trilobatus*. PLoS One 10 (5), e0128108.
Stow, D.A.V., Faugères, J.-C., 2008. Chapter 13 contourite facies and the facies model. In: Rebesco, M., Camerlenghi, A. (Eds.), Contourites. Vol. 60. pp. 223–256 Developments in Sedimentology.
Stow, D.A.V., Faugères, J.-C., Gonthier, E., 1986. Facies distribution and textural variation in Faro Drift contourites: velocity fluctuation and drift growth. Mar. Geol. 72 (1–2), 71–100.
Stow, D.A.V., Pudsey, C.J., Howe, J.A., Faugères, J.-C., Viana, A.R. (Eds.), 2002. Deep-water contourite systems: modern drifts and ancient series, seismic and sedimentary characteristics. Geol. Soc. Mem. 22 (464 pp).
Stow, D.A.V., Hernández-Molina, F.J., Llave, E., Bruno, M., García, M., Diaz del Río, V., Somoza, L., Brackenridge, R., 2013. The Cadiz contourite channel: sandy contourites, bedforms and dynamic current interaction. Mar. Geol. 343, 99–114.
Stuiver, M., Reimer, P.J., 1993. Extended ^{14}C Data Base and Revised CALIB 3.0 ^{14}C Calibration Program. In: Stuiver, M., Long, A., Kra, R.S. (Eds.), Calibration 1993. Radiocarbon 35 (1), pp. 215–230.
Telford, R.J., Heegaard, E., Birks, H.J.B., 2004. The intercept is a poor estimate of a calibrated radiocarbon age. The Holocene 14, 296–298.
Thiede, J., 1971. Variations in coiling ratio of Holocene Planktonic Foraminifera. Deep-Sea Res. 18, 823–831.
Toucanne, S., Mulder, T., Schönfeld, J., Hanquiez, V., Gonthier, E., Duprat, J., Cremer, M., Zaragosi, S., 2007. Contourites of the Gulf of Cadiz: a high-resolution record of the paleocirculation of the Mediterranean outflow water during the last 50,000 years. Palaeogeogr. Palaeoclimatol. Palaeoecol. 246, 354–366.
Turon, J.L., Lézine, A.M., Denèfle, M., 2003. Land-sea correlations for the last glaciation inferred from a pollen and dinocyst record from the Portuguese margin. Quat. Res. 59, 88–96.
Ujiié, Y., de Garidel-Thoron, T., Watanabe, S., Wiebe, P., de Vargas, C., 2010. Coiling dimorphism within a genetic type of the planktonic foraminifer *Globorotalia truncatulinoides*. Mar. Micropaleontol. 77, 145–153.
Voelker, A.H.L., de Abreu, L., 2011. A review of abrupt climate change events in the northeastern Atlantic Ocean (Iberian margin): latitudinal, longitudinal, and vertical gradients. Abrupt climate change: mechanisms, patterns, and impacts. Geophys. Monograph Series 193, 15–37.
Voelker, A.H.L., Lebreiro, S.M., Schonfeld, J., Cacho, I., Erlenkeuser, H., Abrantes, F., 2006. Mediterranean outflow strengthening during Northern Hemisphere coolings: a salt source for the glacial Atlantic? Earth Planet. Sci. Lett. 245 (1–2), 39–55.
Voelker, A.H.L., de Abreu, L., Schönfeld, J., Erlenkeuser, H., Abrantes, F., 2009. Hydrographic conditions along the western Iberian margin during marine isotope stage 2. Geochem. Geophys. Geosyst. 10, Q12U08.
Weldeab, S., Menke, V., Schmiedl, G., 2014. The pace of East African monsoon evolution during the Holocene. Geophys. Res. Lett. 41, 1724–1732.
Wilke, I., Meggers, H., Bickert, T., 2009. Depth habitats and seasonal distributions of recent planktic foraminifers in the Canary Islands region (29°N) based on oxygen isotopes. Deep Sea Res., Part I 56 (1), 89–106.
Zenk, W., Armi, L., 1990. The complex spreading patterns of Mediterranean water off the Portuguese continental slope. Deep-Sea Res. 37, 1805–1823.